Cape Peninsula
University of Technology

SENSITIVITY ANALYSIS OF EB-PVD THERMAL BARRIER COATINGS FOR AEROSPACE APPLICATIONS

MAXIMILJAN DU PLESSIS

Dissertation submitted in fulfilment of the requirements for the degree
Master of Technology: Mechanical Engineering
in the Faculty of Engineering
at the Cape Peninsula University of Technology

Supervisor: Dr N Mahomed

Co-supervisor: Dr A Nowotnik

September 2014

DECLARATION

This dissertation is part of a double degree programme between the Faculty of Engineering of Cape Peninsula University of Technology (South Africa) and the Faculty of Foundry Engineering of AGH University of Science and Technology (Poland).

As part of the programme, the student completed the following courses at Cape Peninsula University of Technology:

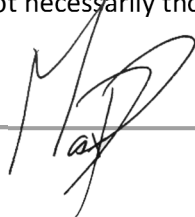| |
|---|
| COURSEWORK:
STL500S: Continuum Mechanics and Intro to Finite Element Analysis
MTD500S: Metallurgical Thermodynamics |
| COMPUTER AIDED DESIGN:
Introduction to CATIA. One-week training programme at the Product Lifecycle Management Competency Centre, CPUT. |
| PATTERN MAKING IN FOUNDRY TECHNOLOGY:
Principles of additive manufacturing and rapid prototyping. Rapid Pattern-Making of wax models for sand and investment casting. One-week programme conducted at the RPD Laboratory, University of Stellenbosch. |
| FOUNDRY TECHNOLOGY: SAND CASTING: Principles of Sandcasting. One-week internship programme conducted at Atlantis Foundries. |
| FOUNDRY TECHNOLOGY: INVESTMENT CASTING: Physical Aspects of Castings (Mould, Production, Materials, Solidification of Metals); Wax room process review (Wax room operations, Materials, Production work); Ceramic Shell room review (Shell room operations, Materials, Production work); Melting and casting review (Ceramic mould preparation, Ferrous and non-ferrous melting, Spectrographic analysis and casting). One-week programme conducted at the CASTCO Foundry. |
| SIMULATION OF CASTING PROCESSES: Introductory course on the use of MAGMASOFT: Process Modelling; Mesh Generation; Process Simulation. |
| Eight-week Product Design and Simulation project using CATIA and MAGMASOFT. |

As part of the programme, the student completed the following courses at AGH University of Science and Technology:

Coursework:	ECTS
Mathematics for Engineers	3
Thermodynamics of Alloys	3
Theory of Foundry Processes	3
Physical Chemistry of Metallurgical and Foundry Processes	3
High Quality Iron Alloys	2
Nonferrous Alloys for Special Applications	2
Metal Matrix Composites	2

Metal Forming Products	3
Powder Metallurgy Products	2
Designing of CAMD Products	2
Finite Difference Methods	3
Applying CAD Systems for Design Casting Technology	2
Foreign Language (special)	3
Theory of Elasticity and Plasticity	3
Iron Alloy Castings	2
Nonferrous Alloy Castings	2
Numerical Simulation and Experimental Methods for Mechanical Characterisation of Solids	4
Computer Networks and Clusters	2
Applying Computer Methods to Optimise a Cast Strength	2
Object Oriented Programming and Database Programming	2
Design and Application of Advanced Engineering Materials	2
Multi-scale Modelling	2
Precision Casting Technology	2
Computer Aided Tooling Manufacturing for Foundry Engineering	2
Elective Course I: Casting Technology Design	1
Elective Course I: Developing Quality of the Surface Layer of Castings	1
Metrology of Foundry Processes	1
Art Casting Technology	2
Selected Aspects of Corrosion in Cast Materials	2
Designing of Information Systems for Production Management in Foundries	1
Numerical Simulation and FEM	3
Seminar	1
Project	10

I, Llewellyn Heinrich Cupido, declare that the contents of this dissertation represent my own unaided work, and that the dissertation has not previously been submitted for academic examination towards any qualification outside of the double degree programme. Furthermore, it represents my own opinions and not necessarily those of the Cape Peninsula University of Technology.

15 September 2014

_____   _____
Signed   **Date**

ABSTRACT

Thermal Barrier Coatings (TBC's) created by Electron Beam Physical Vapour Deposition (EB-PVD) are widely used in the aerospace industry. Advancements in the field however are hindered by the cost and time required for research and development. Hence, there exists a need for a more comprehensive understanding of coating parameter interactions to better predict response values without the need for extensive pre-production testing.

This thesis seeks to provide a response surface for EB-PVD coatings, by investigating the following EB-PVD independent input variables: electron beam emission current, gas ratio, vacuum pressure, substrate temperature, roughness and process time in order to generate a predictive statistical model. Output variables were numerous, however emphasis was placed on: TBC coating thickness and density of columns generated during the process. It is impossible to select an "optimum process recipe"; rather, there exists many optimal combinations suited to specific coating structure and its application. Therein lies the need for this model, able to predict TBC properties according to input variables.

Using ALD's Smart Coater (ALD Vacuum Technologies GmbH), a ceramic top coat (Yttria partially stabilized zirconia, YPSZ, ZrO_2-7%Y_2O_3) was deposited onto 40x30x5mm Inconel 617 samples with NiAl bond coat. These samples were subsequently tested to determine coating properties. The research will show that the complex nature of EB-PVD TBCs may be simplified, at least to a certain degree through a statistical analysis of the interactions between process variables.

Table of Contents

1 - Acknowledgments

I would like to express a deep sense of gratitude to D.Sc. Eng. Jan Sieniawski, Ph.D. Eng. Andrzej Nowotnik and M.Sc. Sławomir Kotowski for the opportunity to gain such valuable knowledge in the field of aerospace materials and for always going above and beyond my expectation to involve me in projects and training at the laboratory, also to the rest of the staff at the Research and Development Laboratory for Aerospace Materials at Rzeszow University of Technology, Ph.D. Nawaz Mahomed of the Cape Peninsula University of Technology, Prof. Jacek Rońda of AGH as well as everyone not mentioned here, for their assistance and support during the completion of this thesis.

A special thanks to my closest friends and family for their unwavering support over the course of this program. Also to Sandy and Helga, thank you for all the challenges.

2 - Introduction

Thermal Barrier Coatings (TBCs) are described as low conductive heat resistant physical barriers generally composed of a ceramic composite that lies above a bond-coat and substrate material. The purpose of the bond-coat is to act as an adhesive between the top-coat and substrate material, the top-coat in turn is able to accommodate thermal expansion differences between the layers (Schulz, Munawar, & Mechnich, 2012). Falling within the "thin films" classification, TBCs range from a few μm to many mm thick (see Figure 1 below). The aim of a TBC is to create a high temperature gradient between the coated substrate and the operating atmosphere over a sustained period of time, thus limiting or completely mitigating the effects of wear, creep and fatigue (Avallone, Baumeister, & Sadegh, 2007).

YSZ Top Coat (0.1-3mm)
- Low thermal conductivity
- High Strain Compliance
- Extreme temperature Gradient

Bond Coat (30-100μm)
- Aluminium Reservoir for formation of protective Al2O3.
- Interdiffusion zone between sub strate and YSZ.
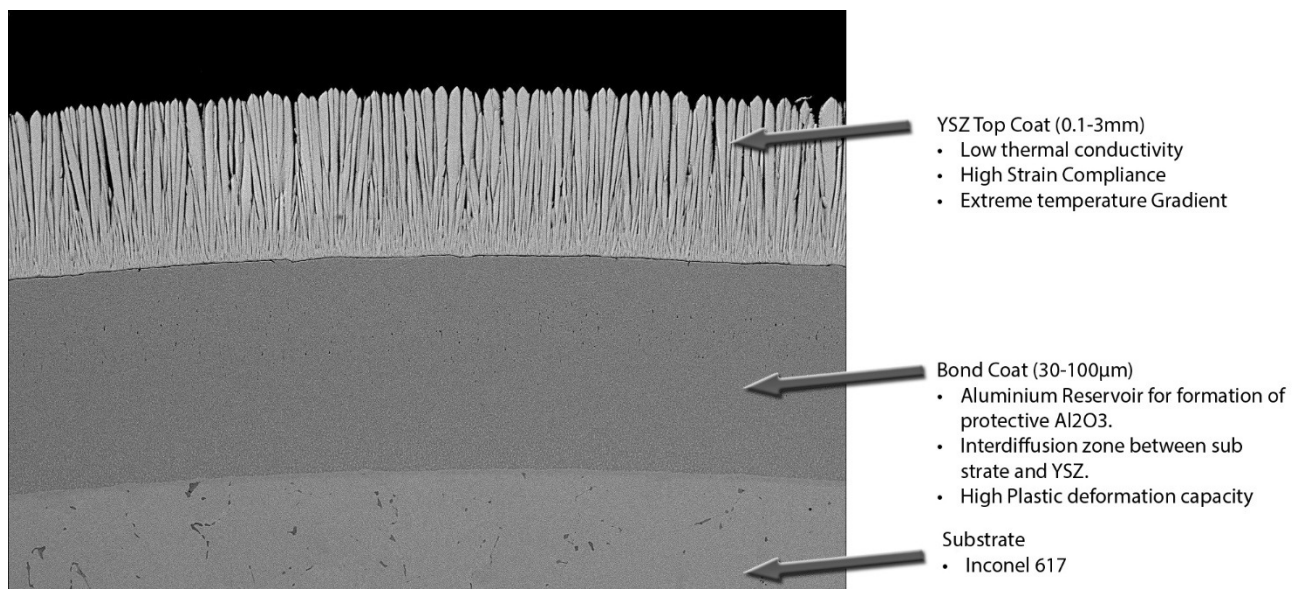- High Plastic deformation capacity

Substrate
- Inconel 617

Figure 1 Illustration of the multi-layered structure of a thermal barrier coating (TBC) system. The ceramic topcoat is deposited by Electron Beam Physical Vapour Deposition (EB-PVD) or air plasma-spraying (APS).The substrate material can be seen below (Research and Development Laboratory for Aerospace Materials, 2014).

The first semi-successful aerospace ceramic coating, known as the NBS Frit Enamel coating, detailed in a paper by Harrison and Moore in 1947 (Miller, 2009), proved that ceramics could extend the lifespan of turbine blades; however, poor results obtained from tests conducted by the US Air Force between the 40'-s and 60'-s stunted the development of these coatings. In 1960, the X-15 Rocket built in the US for super-sonic flight tests successfully used parts coated with a ceramic coating known as Rokide™ (Miller, 2009). Since then, Thermal Barrier Coatings and their bond-coat counter parts have seen massive developments (Cosack &

Schultz, 2012). Current limits are being set by TBCs deposited via Electron Beam Physical Vapour Deposition onto turbine components in both the military and civilian aviation sectors.

Figure 2: Airbus A380, currently the largest passenger plane in the world, featuring four Rolls Royce Trent 970 turbofans. Hot zone components are coated with zirconia based ceramics, allowing them to run more efficiently with less cooling at a higher operating temperatures (<1400 °C) (Airbus. 2014).

The following thesis describes all research steps completed towards establishing a response surface for Electron Beam Physical Vapour Deposition (EB-PVD) process and basic properties of high temperature resistant and thermally insulating coating widely applied for hot section aircraft engine components. These include establishing a preparation procedure for deposition of each layer of TBC coating and for microscopic observations of coating microstructure. The author explains the problems associated with both procedures and documents the process in which a suitable methodology was developed.

The relationship between surface roughness of substrate and bond-coat was analysed in an attempt to ascertain whether the effect on Chemical Vapour Deposition (CVD) could be attributed to this parameter; conclusions are drawn at the end of this section. Below is the schematic of typical duplex structure of CVD\EB-PVD TBC coating with metallic bond-coat and ceramic, columnar top-coat deposited on a nickel superalloy substrate. Analysis of this coating is one of the main research objectives in this study. Understanding the relationships between process variables is key to being able to customize, maximise and predict the thermal gradient shown by the black contour line in Figure 3 below.
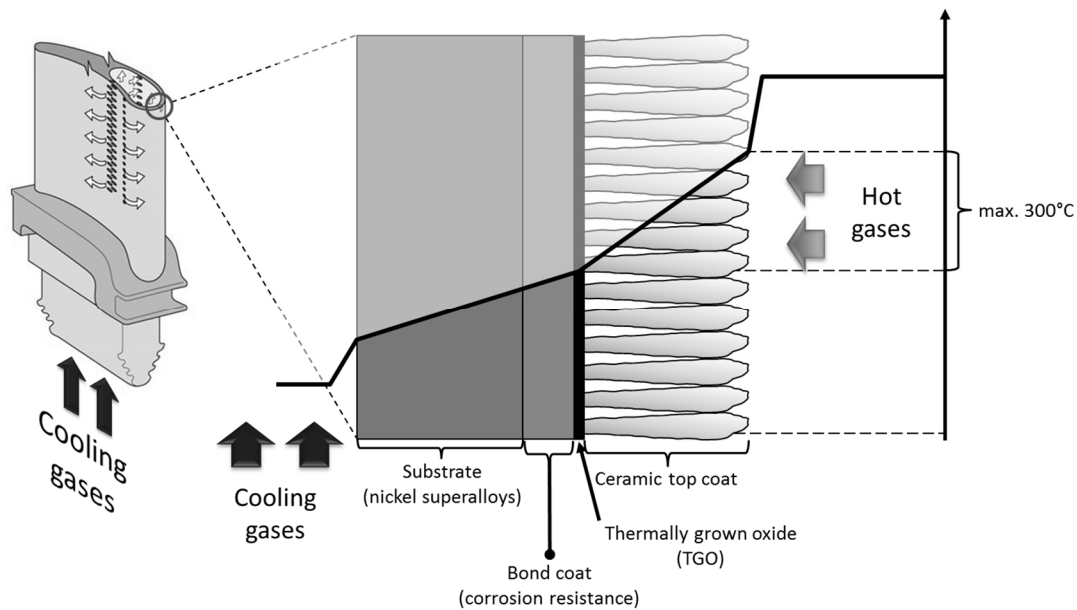
Figure 3: The diagram above shows the typical, duplex structure of CVD\EBPVD TBC coating with metallic bon-coat and ceramic, columnar top-coat deposited on the nickel super-alloys (Slawomir, 2013).

The vapour plume intensity was analysed in order to determine an estimated thickness distribution profile in the coating area obtained during the EB-PVD process. It is important to establish a thickness variance throughout the working area, in particular the difference between coating deposited on samples mounted on different feeder fixtures.

Before the process modelling began, boundary limits for each analysed process input parameter had been established (explained in Chapter 5.6). The obtained process data were applied to the development of a statistical model based on Response Surface Methodology (RSM). This process will be discussed and relationships between machine input variables and coating environment will be shown.

The final statistical model of the EB-PVD process, correlating the process parameters with basic characteristics of TBC top-coat, was created and verified based on analysis of twenty four flat Inconel 617 samples and 12 cylindrical Inconel 617 samples which were coated with duplex CVD-NiAl/EB-PVD-YPSZ Thermal Barrier Coating. During this analysis, column density, coating condition and coating thickness were examined using regression modelling. Finally, conclusions about the model and variables will be drawn together with recommendations for future work and possible improvements to the model.

3 - Research objectives

The primary aim of this research is to investigate the effects of all relevant input variables (e.g. working pressure in coating chamber, argon to oxygen gas flow ratios, emission current of electron beam, coating time, etc) in the deposition of yttria partially stabilized zirconia (YPSZ, ZrO_2—$7\%Y_2O_3$) top-coat via EB-PVD on various sample substrates that are initially bond-coated with nickel aluminide (NiAl). The final result will be a statistical model based on Response Surface Methodology (RSM) and regression modelling providing the relationships between input and output variables required for accurate predictions of future coating processing. Analytical methods suffer from large deviations between calculated and practical results (Vaidyanathana, Jordan, & Maurice, 2004); a statistical approach mitigates material phenomena which may cause these deviations such as faults in coating due to inconsistent input variables.

3.1 Steps completed during research

Sample design and manufacture – Sample materials were machined into predefined sizes (see Appendices D) for use in the ALD Smart Coater™. Sample holders were designed and manufactured to hold the samples without shadowing effect, which would affect the coating thickness and microstructure.

1.   Samples preparation before first deposition process:

The current research was conducted on twelve cylindrical samples (Inconel 718) and twenty four flat specimens (Inconel 617). The surface of each sample was automatically polished to various roughness's between (0.1µm & 2µm) before deposition of the first layer – the metallic bond-coat. Cylinder-shaped samples were polished with variable speed grinding/polishing machines - Struers TegraPol-25+TegraForce-5+TegraDoser-5 (See Figure 15). Since the geometry of flat specimens made the same polishing method problematic due to sharp edges constantly snagging the polishing paper, the Avalon TE-18 centrifugal tumbler (Figure 38) was applied. Before the deposition process of the first layer, all samples were cleaned in an ultrasonic cleaner in high-purity isopropyl alcohol.

2.   Bond-coat deposition process (CVD):

All samples were subjected to a Chemical Vapour Deposition (CVD) process in order to obtain the first nickel aluminide (NiAl) layer (also referred to as the bond-coat). Cylindrical samples (Inconel 718) were used for the preliminary study of surface roughness.

3.   Samples preparation before second deposition process:

All flat Inconel 617 samples were cleaned in an ultrasonic cleaner in high-purity isopropyl alcohol.

4.   Top-coat deposition process (EB-PVD):

a. Thirty one 5min-long processes were performed in order to establish an optimal coating window and correlate process parameters (working pressure in coating chamber, process gases flow ratio, emission current, ingot feed rate).

b. In order to determine the vapour intensity variation and coating thickness distribution within the ceramic vapour plume formed during the EB-PVD process, a stainless steel wire mesh (AISI314) was deposited with the ceramic coating.

c. Twenty four flat Inconel 617 samples were coated with ceramic YPSZ top-coat during the EB-PVD process.

5.   Sample analysis:

a. For cylindrical samples, the correlation between roughness of substrate (before CVD process) with bond-coat roughness after the process was analysed using a Hommel 8000 Suface measurement device (Figure 21). These results were used to assess if the post-CVD roughness fell into the optimal range required for top-coat deposition.

b. The wire mesh was cut, mounted and submitted to observation to determine the coating distribution and ceramic vapour intensity profile in the deposition area.

c. For the flat samples with full structure of TBC coating, the roughness of the top-coat surface was measured. Afterwards, specimens were prepared for microscopic investigations; samples were mounted, cut and polished according to the developed procedure (see Table 3). Grinding papers, polishing discs, lubricants and duration of each of the polishing stages were determined in order to preserve the columnar structure of the ceramic top-coat during the process.

6.   Statistical model:

The statistical model was the final part of the research. Using Statistics made it possible to establish correlation between the parameters of the EB-PVD process and between the parameters and basic characteristics of the top-coat. All statistical analyses in the current study were carried out with the use of Design-Expert© software (version 8.0.7.1).

3.2 Research Methodology
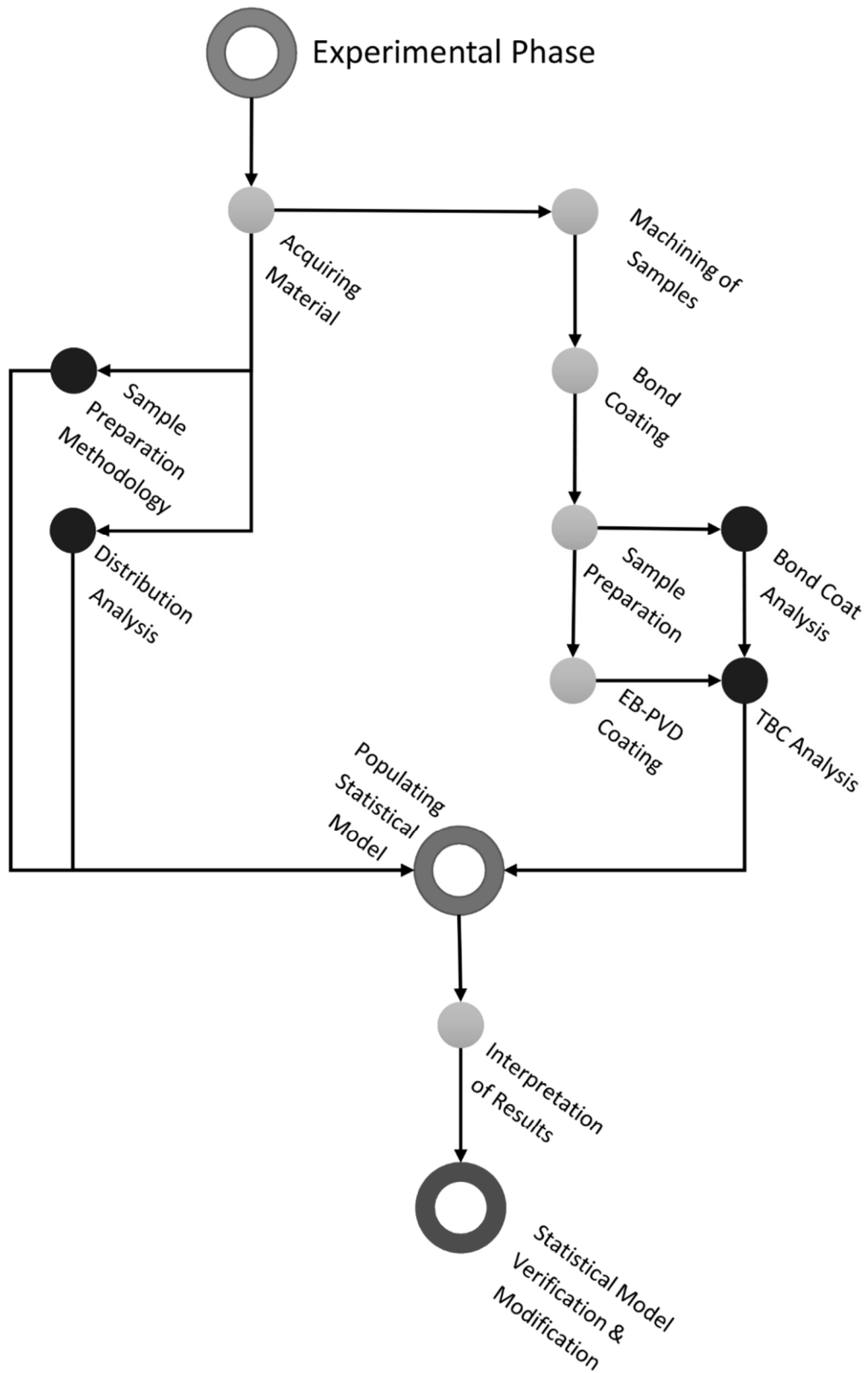
4 - Literature review

4.1 Thermal Barrier Coatings (TBCs)

Thermal Barrier coatings (TBCs) are refractory-oxide ceramic coatings applied to the surfaces of components in the hottest areas of turbine engines, enabling modern engines to operate at significantly higher gas temperatures than their predecessors (Clarke, Oechsner, & Padture, 2012). TBCs provide thermal insulation for metallic components from combustion gasses, allowing a reduction in the substrate temperature between 100 °C to 300 °C in 120µm to 400µm thicknesses (Osorio, Toro, & Hernandez-Ortiz, 2012). Higher temperatures of inlet gases relate to higher efficiencies in the turbine (see Figure 4).
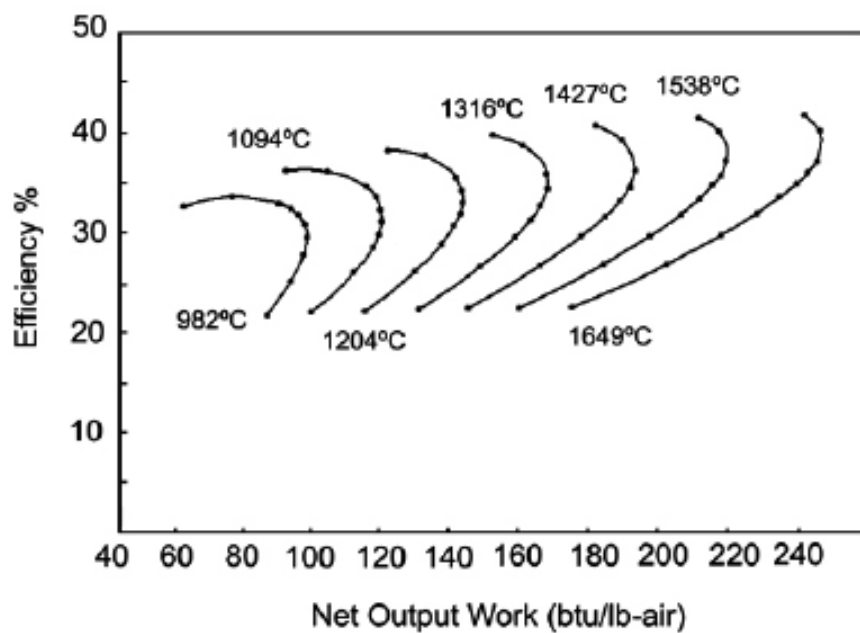

Figure 4 Efficiency increments with an increase in service temperature (Osorio, Toro, & Hernandez-Ortiz, 2012).

4.2 Chemical Vapour Deposition (CVD) process

The Chemical Vapour Deposition (CVD) process involves the chemical reaction of gaseous reactants on or in the vicinity of a heated substrate surface. This atomistic deposition method can provide highly pure materials with structural control at atomic or nanometer scale level (Choy, 2000).. Moreover, it can produce single layer, multilayer, composite, nanostructured, and functionally graded coating materials with well controlled dimension and unique structure at low processing temperatures. Furthermore, the unique feature of CVD distinguishing it from other techniques, such as the non-line-of-sight-deposition capability (Sun, Lin, & Hon, 1986), has allowed the coating of complex shaped engineering components. It is used together with refractory ceramic materials (e.g. SiC, TiN, TiB_2, Al_2, O_3, BN, $MoSi_2$, ZrO_2) used for hard coatings, protection against corrosion and oxidation or as diffusion barriers (Choy, 2000).

Chemical Vapour Deposition (CVD) involves a chemical reaction to synthesize a material, such as Nickel-Aluminium (NiAl), as it is deposited over the substrate. This process is often carried out in batches in high-temperature furnaces with a controlled flow of reactants and at low or atmospheric pressure (Avallone, Baumeister, & Sadegh, Marks' Standard Handbook for Mechanical Engineers Eleventh Edition, 2007). The chemical reactions for CVD can also be plasma enhanced (PECVD), This provides the capability of performing the deposition process at lower temperatures, good control of the film properties, and high deposition rates, but requires expensive serial processing (Avallone, Baumeister, & Sadegh, Marks' Standard Handbook for Mechanical Engineers Eleventh Edition, 2007).

Nickel-based super alloys need to be given aluminizing treatments to provide a barrier coating when they are used in environments which are known to cause severe surface degradation. The aluminizing process results in the formation of nickel aluminide phase layers on the alloy surface which can provide improved corrosion and oxidation resistance, thereby enhancing the service life and reliability of the coated alloy (Sun, Lin, & Hon, 1986).

4.3 Advantages of Chemical Vapour Deposition (CVD)

CVD has several important advantages which makes it the preferred process in many cases. These are summarised as follows (Pierson, 1999):

- It is not restricted to a line-of-sight deposition which is a general characteristic of sputtering, evaporation and other PVD processes. As such, CVD has high throwing power. Deep recesses, holes and other difficult three-dimensional configurations can

usually be coated with relative ease. For instance, integrated circuit via holes with an aspect ratio of 10:1 can be completely filled with CVD tungsten (Pierson, 1999).

- The deposition rate is high and thick coatings can be obtained (in some cases centimetres thick) and the process is generally competitive and, in some cases, more economical than the PVD processes (Pierson, 1999).

- CVD equipment does not normally require ultra-high vacuum and generally can be adapted to many process variations. Its flexibility allows many changes in composition during deposition and the code position of elements or compounds is readily achieved (Pierson, 1999).

CVD however, has several disadvantages. A major one being that it is most versatile at temperatures of 600°C and above; many substrates are not thermally stable at these temperatures. However, the development of plasma-CVD and metallo-organic CVD partially offsets this problem. Another disadvantage is the requirement of having chemical precursors (the starter materials) with high vapour pressures which are often hazardous and at times extremely toxic. The by-products of the CVD reactions are also toxic and corrosive and must be neutralised, which may be a costly operation (Pierson, 1999). The primary disadvantage of CVD coatings is their lack of thickness and consequent low wear and crater resistance. Typical CVD coated inserts have coating thicknesses ranging from 10μm to 20mm supplementing this disadvantage of PVD coatings which may be 2.5 μm to 4 mm thick (Avallone, Baumeister, & Sadegh, Marks' Standard Handbook for Mechanical Engineers Eleventh Edition, 2007).

In many respects, CVD competes directly with the PVD processes, but it is also used in conjunction with them, and many of the newer processes are actually combinations of the two systems such as plasma enhanced CVD or activated sputtering (Pierson, 1999).

4.4 Roughness requirements between bond-coat and top-coat

From a mechanical perspective, an increase in surface roughness also increases surface area and thus adhesion force. However, during thermal expansion, high shear causes more inelastic deformation in the constituent materials, or promotes near-tip sliding against roughness, propagating into thermal fatigue cracking if the interface roughness is higher than 2μm (Sou, 2002).

4.5 Electron Beam Physical Vapour Deposition (EB-PVD)

The industrial application of Electron Beam Physical Vapour Deposition process in the deposition of Thermal Barrier Coatings (EB-PVD TBCs) on turbine parts started in the 1970s. A concept of a production EB-PVD coater was soon developed. The breakthrough in development of TBCs on turbine blades for aero engines succeeded at the beginning of the 1980s. Since the beginning of the 1990s, hardly no newly designed jet engine can be found without an EB-PVD TBC on high pressure turbine aerofoils. It created a need to introduce mass production of EB-PVD coatings with hundreds of thousands of turbine components per year (Cosack & Schultz, 2012).

The EB-PVD deposition of ceramic coatings is a complex process conducted in a vacuum chamber at temperatures up to approximately 1100°C. The EB-PVD processing relies on evaporation of a material, utilising a high vapour pressure over a molten ceramic ingot. The electron beam is generated and shaped in the electron beam gun (see Figure 5). It is focused on the surface of the ceramic ingot. The ceramic material is evaporated at a temperature of approximately 2700°C (Sampath, Schultz, Jarligo, & Kuroda, 2012). During the coating process, the preheated samples mounted on the feeder are moving in the ceramic vapour cloud. The vapour is deposited onto the substrates at the rate of approximately 6µm/minute (data for SMART Coater). To achieve a defined stoichiometry of the zirconia, oxygen is bled into the deposition chamber to compensate for the deficit caused by dissociation (Sampath, Schultz, Jarligo, & Kuroda, 2012). Rotation of the parts is mandatory if the substrates or blades need to be coated on all sides. Owing to the formation of the coating from the vapour phase and combined actions of shadowing and crystallographic growth selection, a columnar microstructure of the TBC can be achieved, providing a high level of strain tolerance. To ensure continuous growth of the ceramic coating, cylindrical ingots of the ceramic are bottom-fed into the crucibles pool (Sampath, Schultz, Jarligo, & Kuroda, 2012).
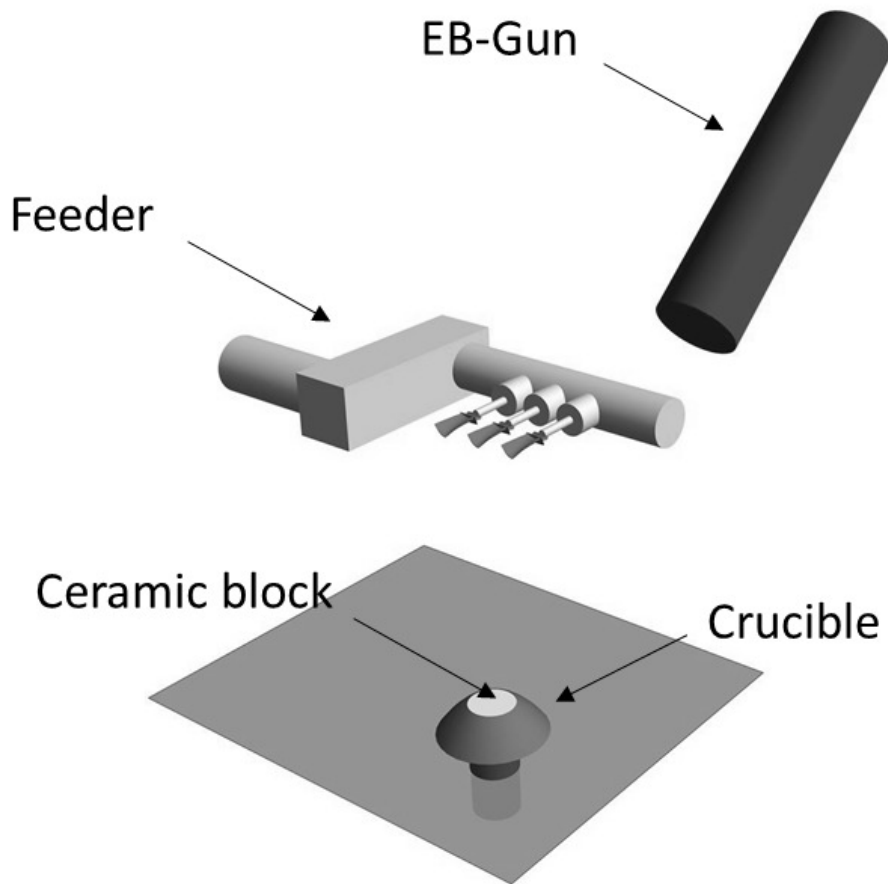
Figure 5 Schematic of EB-PVD coating chamber (Slawomir, 2013).

Formation of the microstructure of EB-PVD TBCs is closely related to process conditions. Since shadowing occurs primarily along the plane of vapour incidence, columns are significantly wider in the direction parallel to the rotation axis than perpendicular to it, leading to an anisotropy of the in-plane compliance with notable consequences to the strain tolerance of the coating (Sampath, Schultz, Jarligo, & Kuroda, 2012).

4.6 Advantages of EB-PVD process

Favourable characteristics of EB-PVD compared with other coating processes such as plasma spraying include the following (Sampath, Schultz, Jarligo, & Kuroda, 2012):

- EB-PVD coatings have longer life in severe conditions compared with plasma sprayed coatings because of the denser columnar microstructure of EB-PVD and improved mechanical bonding with the substrate.
- EB-PVD TBCs are much smoother in as-deposited state (1.4 to 1.5 µm versus 5 µm as in the case of plasma sprayed coating).

- EB-PVD TBC's taper very rapidly at the openings of the cooling holes in turbines, whereas plasma spray coatings have a tendency to develop a build-up and block the small holes.
- It is more economical when a number of parts are coated simultaneously.
- It is more preferable than Chemical Vapour Deposition (CVD) for coating temperature-sensitive components since CVD is a high-temperature process.

Unlike the CVD process which have chemical precursors with high vapour pressure which are often hazardous and at times extremely toxic, the EB-PVD process is relatively environmentally friendly (Pierson, 1999).

4.8 Yttria partially stabilized zirconia

Yttria partially stabilized zirconia (YPSZ, ZrO_2—7%Y_2O_3) is the most widely used TBC material today (Cosack & Schultz, 2012). It has been found that addition of 6 to 10 wt.% Y_2O_3 provides TBCs with good thermal and mechanical properties. The purpose of introducing yttria is to stabilize zirconium oxide at room temperature (Osorio, Toro, & Hernandez-Ortiz, 2012). YPSZ has a melting point approaching or in excess of 2427°C, making both processing and evaporation difficult.

Yttria Partially Stabilized Zirconia (YPSZ) is well known as an oxygen ion conductor at elevated temperatures and is practically used as it has almost the same thermal expansion coefficient over the whole temperature range used (Hayashi, Saitou, Maruyama, Inaba, & Kawamura, 2005).

4.7 Inconel 617

Inconel 617 (UNS N06617/W.Nr. 2.4663a) is a solid-solution, strengthened, nickel-chromium-cobalt-molybdenum alloy with an exceptional combination of high-temperature strength and oxidation resistance. The alloy also has excellent resistance to a wide range of corrosive environments, and it is readily formed and welded by conventional techniques. The combination of high strength and oxidation resistance at temperatures over 980°C makes INCONEL alloy 617 an attractive material for such components as ducting, combustion cans and transition liners in both aircraft and land-based gas turbines (Special-Metals, 2014).

Table 1 Inconel 617 Properties according to Special Metals Group (Special-Metals, 2014).

Inconel alloy 617 Properties	
Density (kg/m^3)	8360
Melting Range (°C)	1332 – 1380
Specific Heat (J/Kg.K)	419
Thermal Conductivity at 1000 °C (W/m^2)	28.7
Yield Strength (MPa)	318
UTS (MPa)	734

4.9 Statistical modelling

Bill Pelham once said "Figures can't lie, but liars sure can figure" (Berger & Casella, 2001); Plato argued that statistics was a fuzzy logic; however, it is the chaotic nature of statistics that allows it to accurately represent reality when derived competently. All science relies on some form of statistics to verify theories and often to develop coefficients to mitigate the effect of calculation anomalies.

Statistics can be summarised as set of mathematical procedures for summarising and interpreting observations. These observations are typically numerical or categorical facts about specific people or processes, usually referred to as data. The most fundamental branch of statistics is descriptive statistics, that is, statistics used to summarise or describe a set of observations (Berger & Casella, 2001).

Every hypothesis test contains two hypotheses. The first hypothesis is called the null hypothesis, denoted H_o. The null hypothesis always states that the population parameter is equal to the claimed value, the second (or alternative) hypothesis, denoted H_a (Rumsey, 2011). The standard deviation from this will determine where the theory is proved or rejected. The statistical equivalent of the principle of reasonable doubt is the alpha level agreed upon by most statisticians as the reasonable standard for rejecting the null hypothesis. In most cases, the accepted probability value at which alpha is set is .05%. Even if a study is perfectly executed with no systematic design flaws, it is always possible that the researcher's results were due to chance. In fact, the probability (*p*) value we observe in an experiment tells us exactly how likely it is that we would have obtained results like ours even if nothing but dumb luck more formal maybe "entirely relying on chance" or sth like that) were operating in our study, resulting in incorrectly rejecting the null hypothesis when it is, in fact, correct—this is a

type I error. Thus we set a low α value, however type II error occurs when we fail to reject an incorrect null hypothesis—that is, when we fail to realize that our study has revealed something meaningful (usually that our hypothesis is correct) due to an excessively small α value (Berger & Casella, 2001).
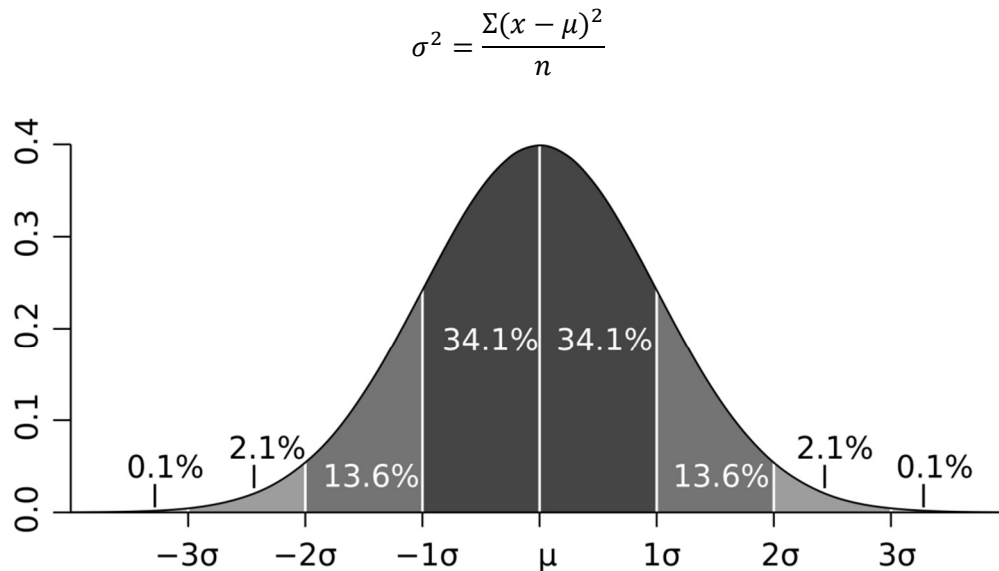
$$\sigma^2 = \frac{\Sigma(x - \mu)^2}{n}$$

Figure 6 Standard Deviation Model (Kemp, 2014).

A chi-square (χ^2) test of association is conceptually identical to a phi coefficient (j) because, like phi, this test of association indicates whether two categorical variables are related. In fact, it is very easy to convert a chi-square test of association to a phi coefficient using the simple formula:

$$\varphi = \sqrt{\frac{\chi^2_{obt}}{N}}$$

One-way analysis of variance (one-way ANOVA) is used to assess the reliability (statistical significance) of mean differences between three or more groups. This test is very similar to an independent samples t-test (and shares the same assumption of a normally distributed dependent measure). However, the difference is that a one-way ANOVA controls for the experiment-wise error rate that occurs as all of the many possible comparisons that can be made between specific groups when there are multiple experimental or naturally existing groups (three or more levels of the independent variable).

When the researcher has a clear a reason to expect the various conditions to yield results that follow a specific pattern, the researcher can greatly increase statistical power by conducting a planned comparison based on this specific expectation (Berger & Casella, 2001).

4.10 Response Surface Method (RSM)

Response Surface Methodology (RSM) consists of a group of mathematical and statistical techniques used in the development of an adequate functional relationship between a response of interest y and a number of associated control (or input) variables denoted by $x_1, x_2, ..., x_n$. In general, such a relationship is unknown, but can be approximated by a low-degree polynomial model of the form (Sastry, 2012):

$$y = f'(x) \cdot \beta + \varepsilon,$$

where $x = (x_1, x_2, ..., x_n)$,) is a vector of input variables, $f(x)$ is a vector function of n elements that consists of powers and cross- products of powers of $x_1, x_2, ..., x_n$ up to a certain degree denoted by d ($d \geq 1$), β is a vector of p unknown constant coefficients referred to as parameters and ε is a random experimental error assumed to have a zero mean. This is conditioned on the belief that the equation above provides an adequate representation of the response (Sastry, 2012). In this case, the quantity $f(x) \cdot \beta$ represents the mean response, that is, the expected value of y.
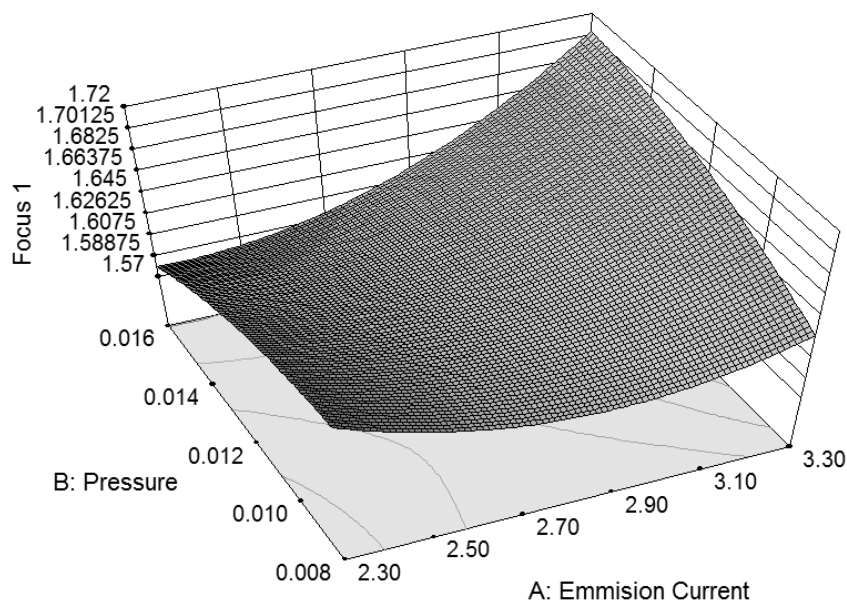
Figure 7 Example response surface generated in Design-Expert© showing Focus 1 value as a function of emission current of electron beam and working pressure in the EB-PVD coating Chamber (M. Du Plesis. 2014).

4.10 Lambert's Cosine Law

The cosine model is used for modelling the shape of the vapour plume generated in EB-PVD because of its simplicity, accuracy and wide acceptance. According to this model, the vapour intensity of the evaporated material can be expressed as (Avallone, Baumeister, & Sadegh, Marks' Standard Handbook for Mechanical Engineers Eleventh Edition, 2007):

$$I(\alpha) = I_0 \cdot cos^n\alpha \left[\frac{kg}{m^2 s}\right]$$

where:

> $I(\alpha)$ - vapour intensity in a direction α degrees from the normal direction to the evaporation source surface,
>
> I_0 - vapour intensity in perpendicular direction to the evaporation source surface,
>
> $n = 2, 3, …, 6$ depends on the rate of evaporation (Schiller model).

The cosine model is valid for a small-area evaporator where the diameter of the melt pool, D_v, is much smaller than the distance between the melt pool and the substrate, h_v. For a flat plate located stationary above the evaporator source and a constant rate of evaporation, the coating thickness over a given period of time has been modelled as (Schiller et al. 1982):

$$\frac{d_s}{d_{so}} = \frac{1}{\left(1 + \left(\frac{r_s}{h_v}\right)^2\right)^{\frac{n+3}{2}}}$$

where:

> d_s - the local film thickness in point of interest,
>
> d_{so} - is the film thickness for $\alpha = 0$,
>
> r_s - the distance on the substrate from the point of maximum thickness,
>
> h_v - is the height of the substrate over the evaporator source.

5 - Experimental work

5.1 Facility and equipment

The Research and Development Laboratory for Aerospace Materials at the Rzeszow University of Technology, was established in 2005 through funding from the Polish Ministry of Education and Science and the European Union. This facility is affiliated with Rzeszow University of Technology's Department of Materials Science and uses the research capacity academic-industry consortium within the "AERONET-Aviation Valley Centre of Advanced Technologies" and a group of aviation-oriented research and training centres, aeronautic producers and suppliers working in the "Aviation Valley Association".

The Laboratory includes an industrial-strength VIMIC 2 E vacuum furnace (ALD Vacuum Technologies GmbH) for DS/SC solidification of nickel super alloys, an EB-PVD SMART Coater (see Figure 8) (ALD) MultiCoat® LPPS® device for plasma spraying under low pressure (Sulzer Metco), a PACVD system for nitriding and nitrocarburizing (Sulzer Metco), a vacuum furnace for carburising, nitriding and nitrocarburising in a nitrogen atmosphere or in vacuum (ALD), a processing centre for studying the influence of high-speed machining, laboratories for sample preparation and microscopic observations of materials, along with many other coating and thin film related equipment.
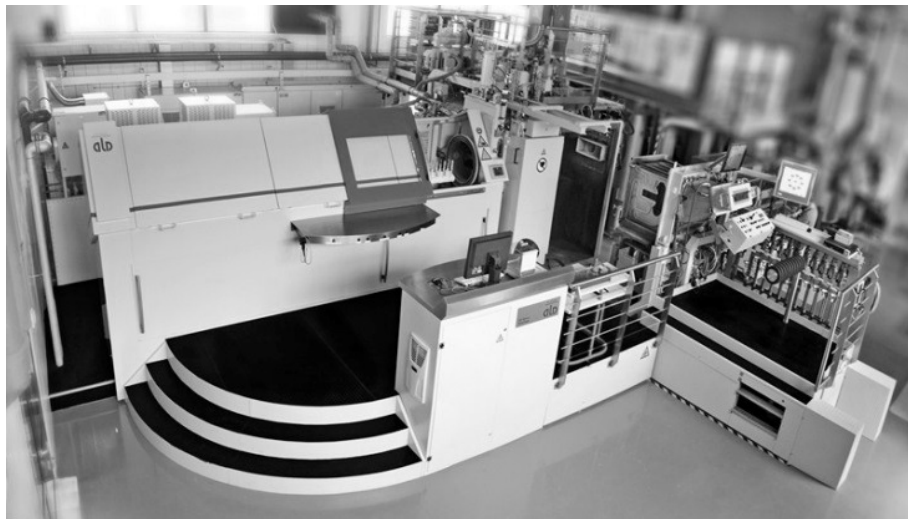
Figure 8 SMART Coater for performing Electron Beam Physical Vapour Deposition Process (EB-PVD) manufactured by ALD Vacuum Technologies GmbH. Research & Development Laboratory For Aerospace Materials (Research and Development Laboratory for Aerospace Materials, 2014).
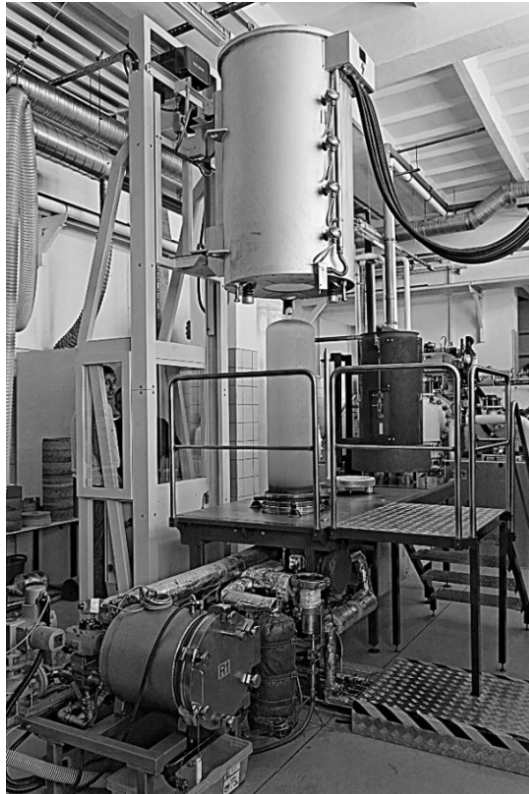
Figure 9 IonBond BPX Pro 325S CVD device for conducting Chemical Vapour Deposition Process (Research and Development Laboratory for Aerospace Materials, photographed by Slawomir Kotowski, 2014).

Figure 10 Metallography Laboratory for performing sample preparation (precision cutting, manual and automatic polishing and mounting) before the coating deposition process, also preparation after the process for microscopic observations. (Research and Development Laboratory for Aerospace Materials, 2014).

Figure 11 Scanning electron microscope HITACHI S-3400 S for high magnification observation (Research and Development Laboratory for Aerospace Materials, 2014).

Figure 12 Metallurgical microscope Nikon EPIPHOT 300 for observation of coating microstructure (Research and Development Laboratory for Aerospace Materials, 2014).

5.2 Research plan

This section describes the steps required and followed for establishing statistical model of EB-PVD process in order to prediction of YPSZ coating properties:

- Development of sample preparation procedure for deposition of each layer of TBC coating.
- The effect of substrate surface roughness on the roughness values of bond-coat and top-coat.
- Defining the operating window for stable evaporation of YPSZ feedstock during EB-PVD process.
- Determining the vapour intensity variation within the ceramic vapour plume formed during EB-PVD process.
- Development of polishing procedure for microscopic analysis of YPSZ columns.
- Microscopic analysis of top-coats.
- Creating the final statistical models which correlates the EB-PVD process parameters and basic characteristics of top-coat.

5.3 Development of polishing procedure

Optical microscopy plays a major role in TBC analysis, therefore the procedure for preparing samples is as important as the analysis itself. Poor sample preparation makes analysis impossible due to column fracture and material removal (see Figure 16).

A series of samples were cut radially into sections (see Figure 13). The samples had the following attributes:

- Substrate: CMSX-4 nickel super alloy, single crystal structure,
- Bond-coat: NiAl coating deposited by Chemical Vapour Deposition (CVD) process,
- Top-coat: Yttria Partially Stabilized Zirconia (YPSZ) coating deposited by Electron Beam Physical Vapour Deposition (EB-PVD) process.

Cutting of the samples required a low vibration method, to avoid TBC damage which may be propagated beyond the polishing depth and affect analysis results. Cutting of samples was carried out on Struers Accutom-50 precision cutting machine (see Figure 13), using a CBN BOC13 cut-off wheel with the parameters shown in Table 2.

Table 2: Cutting parameters for samples on Struers Precision cutter with a CBN BOC13 cut-off wheel

Maximum cutting force	Low
Rotational speed	3200 RPM
Sample approach	Lead-in facing primary TBC surface
Feed rate	0.015 mm/s

Figure 13. Struers Accutom-50 precision cutting machine (Research and Development Laboratory for Aerospace Materials, photographed by Slawomir Kotowski, 2014).

Samples were mounted in DuroFast™ resin before polishing. Initially, each sample was polished with different parameters to reduce the amount of required runs. In order to maintain repeatability, an automatic polisher was used (see Figure 15). After each step, samples which were assessed as relatively well polished (see Figure 17) were used as the baseline for changes to subsequent stages of polishing procedure. It was repeated until a satisfactory microstructure image of top-coat with well-preserved columnar structure was established (see Figure 17).

Figure 14. Fully automatic mounting press for hot mounting Struers LaboPress-3 (Research and Development Laboratory for Aerospace Materials, 2014).

Figure 15. Variable speed grinding/polishing machines Struers TegraPol-25 + TegraForce-5 + TegraDoser-5 (Research and Development Laboratory for Aerospace Materials, photographed by Slawomir Kotowski, 2014).

Table 3: Polishing procedure used for analysis of TBC samples. Specimens were mounted in resin DuroFast™ and polished using central force (see Figure 15)

Procedure X		
Grade	*Time*	*Force*
SiC paper #1000	*A [min]*	*G [N]*
SiC paper #1200	*B [min]*	*G [N]*
SiC paper #2400	*C [min]*	*G [N]*
Diamond paste 6µm	*D [min]*	*H [N]*
Polishing disc MD Mol		
Diamond paste 3µm	*E [min]*	*H [N]*
Polishing disc MD Mol		
Diamond paste 1µm	*F [min]*	*H [N]*
Polishing disc MD Nap		

Assessment: Minimal column degradation

The conclusions drawn during establishing of polishing procedure were:

- Unlike EPOFIX™, inclusion in DuroFast™ prevented damage to column structure and round-off effect during polishing, possibly due to the higher rigidity of this resin.
- Mounting in DuroFast™ is shorter (18min) as opposed to the 12 hour mounting time for EPOFIX™.
- Washing of samples between different diamond paste polishing stages should be done to prevent cross-contamination (each polishing disc should be used with one type of diamond paste) and maintain repeatability.
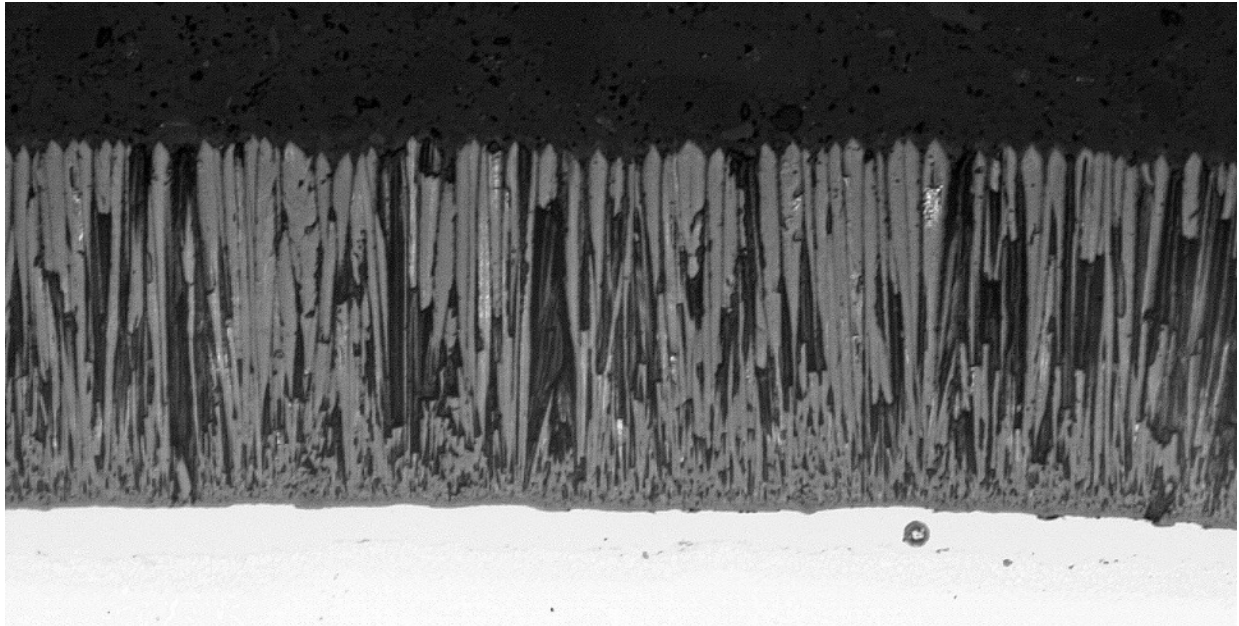
Figure 16 Cross section of YPSZ columns prepared with incorrect procedure, showing severe fracturing.
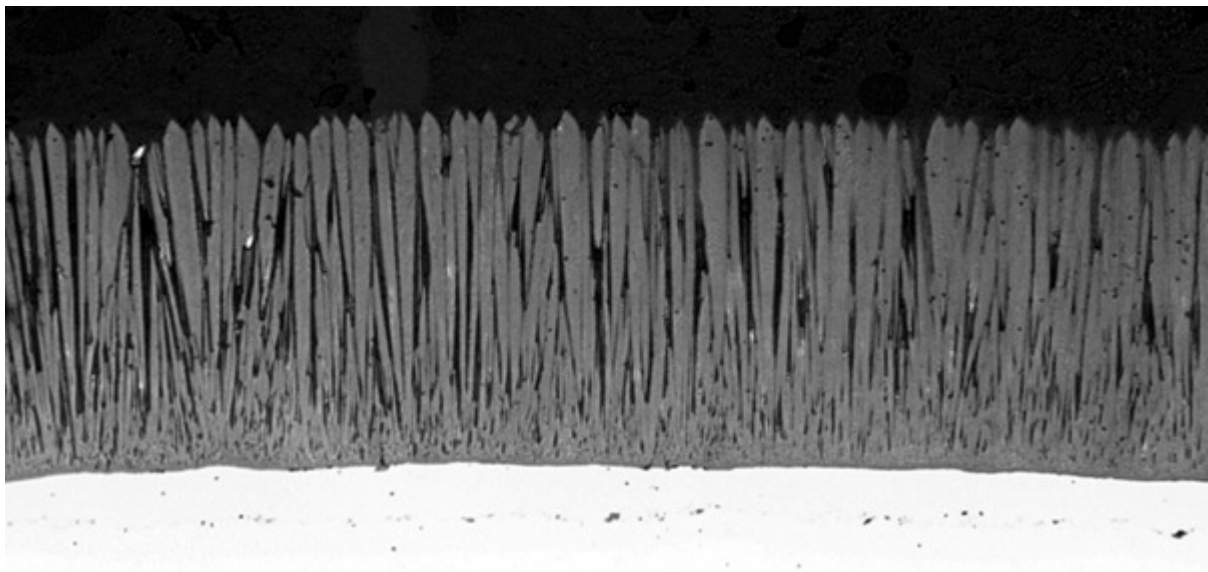
Figure 17. Results of modified polishing procedure to TBC shows clear improvements over the previous one (see Figure 16) above.
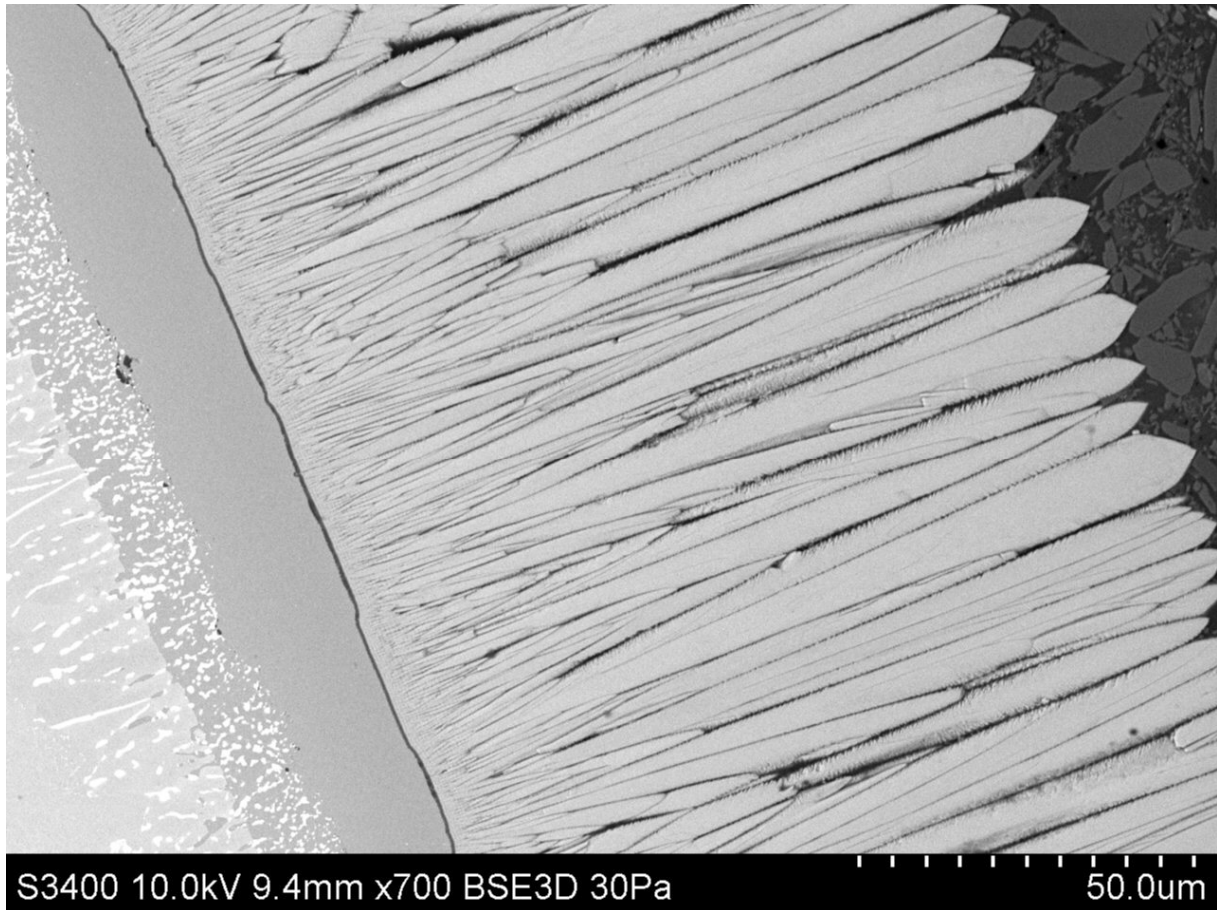
Figure 18. SEM micrograph of TBC structure after using the improved polishing procedure.

5.4 Effects of substrate surface roughness

The roughness of interface between bond-coat and top-coat is significant in determining the life span of a TBC, as this roughness directly relates to thermal expansion allowance (Schulz, Munawar, & Mechnich, 2012). A rough bond-coat prevents top-coat columns from shifting axially during thermal expansion, expediting mechanical failure of the coating. Understanding how to control surface roughness is important for the following reasons:

1. Preparation of substrate is time consuming; thus the most effective methodology should be established to ensure that no redundant work is performed on the samples.

2. To determine if there is an optimal substrate roughness which removes the need for post CVD polishing of bond-coat. EB-PVD requires an R_a value of less than 1.6 µm for successful coating according to industry standards (Schulz, Munawar, & Mechnich, 2012).

In order to generate a broader range of surface roughness values and repeatability of experiment, Inconel 617 samples were polished using a TegraPol-25 automatic polishing machine.
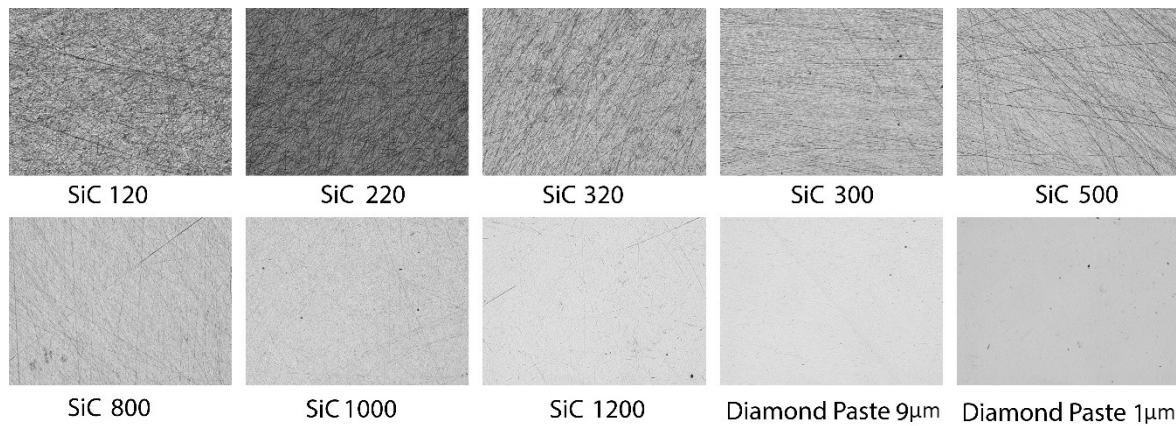
Figure 19 Pictures of sample surfaces after polishing with SiC grinding paper characterised by different grit size and polishing disc with two different diamond pastes.

The roughness (Ra) of the samples were measured using a HOMMEL T8000 roughness and profilometric method (see Figure 20). Automatic polishing provides a uniform polishing pattern on the substrate surface; however, measurements were still taken at two perpendicular directions to ensure generalized measurements. The measurement was classified as successful only if the computer generated profile had no sudden change of values (see Figure 21) and both measurements confirmed that the obtained Ra values are representative for the sample. Otherwise new measurements were taken. In cases when the large results deviation persisted, the sample was re-polished and measured again to give a representative characteristic of surface finish at the given polishing stage.

a)   b)
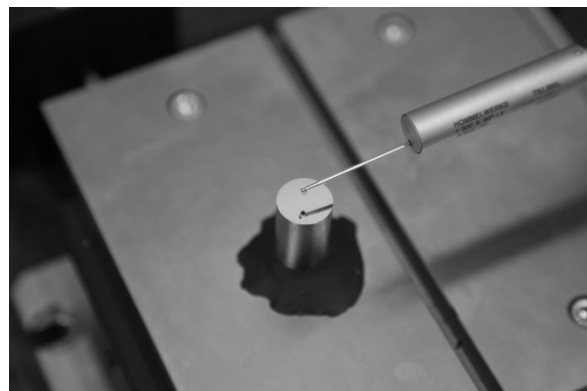
Figure 20 (a) HOMMEL T8000 roughness and contour measuring system and (b) the device probe during roughness measurement (Research and Development Laboratory for Aerospace Materials, photographed by Slawomir Kotowski, 2014).

The three-dimensional surface topology (see Figure 22) can be generated when measuring surface average. However, at higher roughness values, scratches would catch the profile needle and distort the results. Thus, it is better to use a two-dimensional profile for these samples.
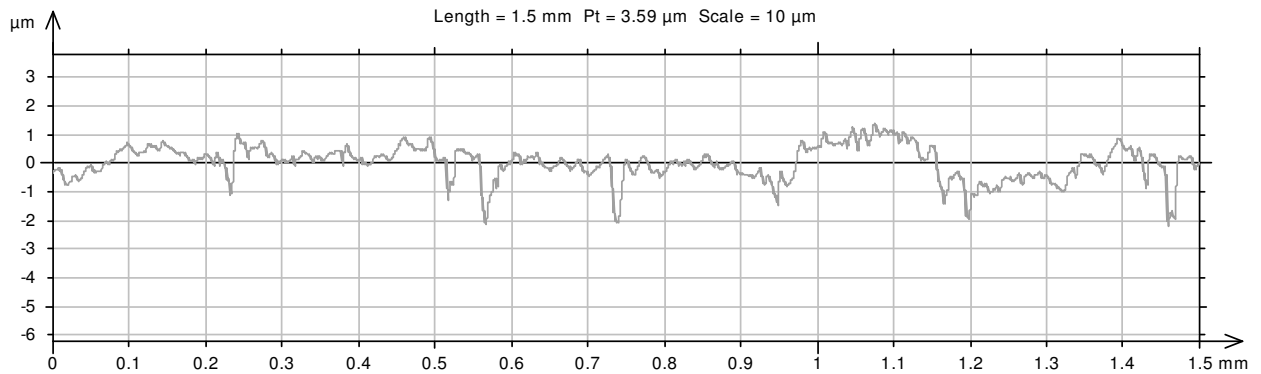

Figure 21. Two-dimensional profile of sample surface generated with the use of HOMMEL T8000 roughness and contour measuring system (see Figure 20), gives a Roughness average (Ra) along a 2D plane.
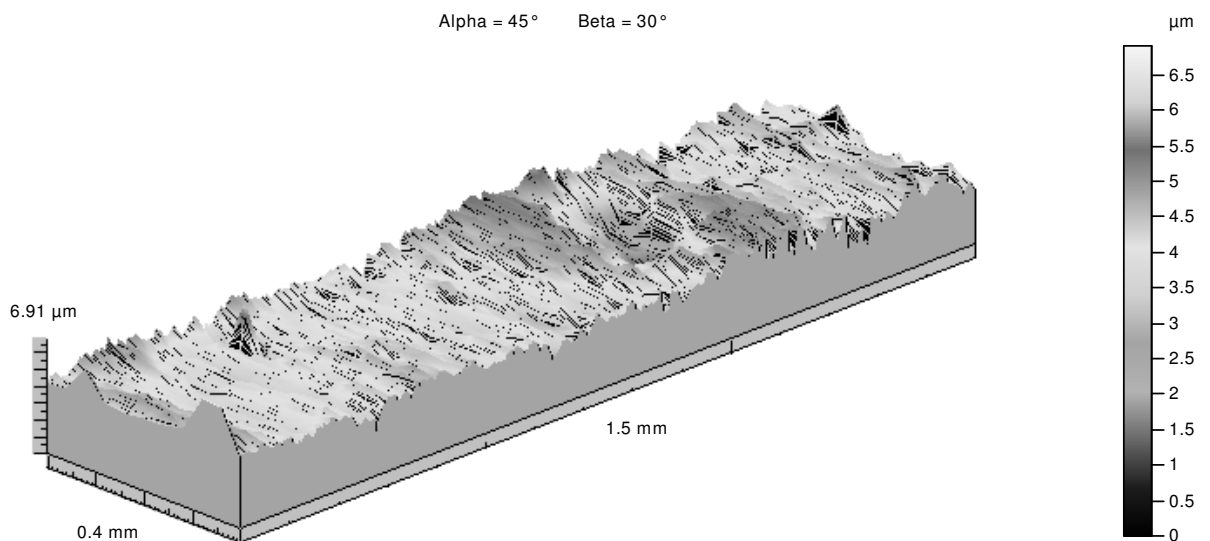

Figure 22. Surface topology generated by HOMMEL T8000 roughness and contour measuring system (see Figure 20) shows defects such as pits and gives a surface roughness average.

After the initial polishing and roughness measurement, samples were coated with nickel aluminide (NiAl) bond-coat using a CVD process. The coating was deposited over a 12-hour period and the consequent surface roughness was measured again, following the same steps as above (see Table 4 and

EB-PVD requires a CVD surface roughness lower than 1.5µm for prolonged lifespan before mechanical failure occurs, often between bond-coat and top coat due to delamination caused by cyclic thermal fatigue. Industry standards specify a bond coat of 1.5 µm; however, bond coat roughness of 0.2 µm has led to significant increases in durability of TBCs & .

).

Table 4: Initial roughness measurements using automatic polishing determined for cylindrical Inconel 718 specimens (see Figure 15). All roughness values are averaged across identical samples.

Media		Inconel 617 Pre-CVD Roughness µm	Inconel 617 Post CVD Roughness µm
120	SiC paper	0.07	1.23
220	SiC paper	0.04	0.96
320	SiC paper	0.04	1.01
500	SiC paper	0.03	1.04
800	SiC paper	0.03	1.14
1000	SiC paper	0.02	1.19
1200	SiC paper	0.02	1.15
2400	SiC paper	0.01	1.30
4000	SiC paper	0.01	1.32
9µm Diamond		0.02	1.19
3µm Diamond		0.02	1.14
1µm Diamond		0.02	1.17

EB-PVD requires a CVD surface roughness lower than 1.5µm for prolonged lifespan before mechanical failure occurs, often between bond-coat and top coat due to delamination caused by cyclic thermal fatigue. Industry standards specify a bond coat of 1.5 µm; however, bond coat roughness of 0.2 µm has led to significant increases in durability of TBCs (Lau, 2003) & (Zhang, Withers, Fox, & Knowles, 1999).
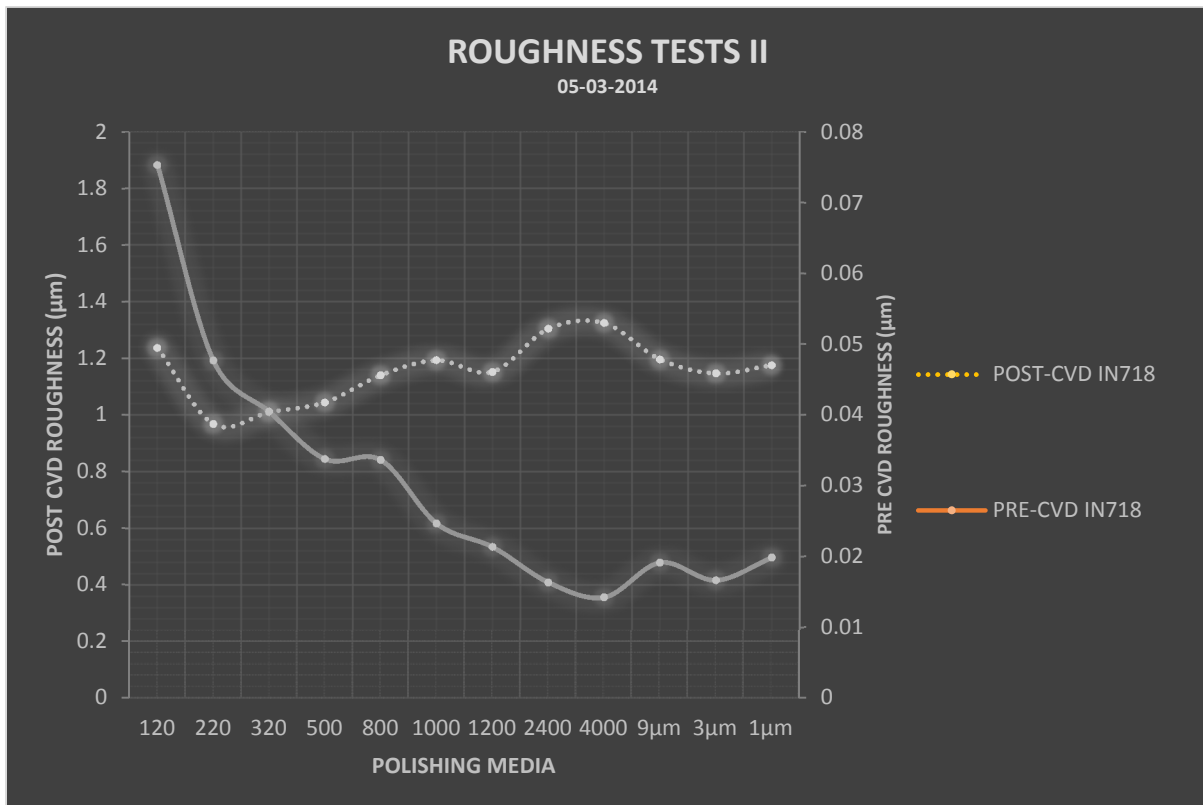
Figure 23 Graph showing results of roughness measurements for cylindrical Inconel 718 samples suggest that effect of substrate roughness on CVD roughness is fairly insignificant.

The insignificant variation of roughness averages between samples before and after CVD process indicated that the substrate roughness has little effect on the CVD roughness and top coat structure. Coating time and emission current are significantly influential when compared to substrate roughness. It seems apparent that more effort should be invested in understanding and controlling these attributes, rather than putting effort into altering the substrate surface.

5.5 Coating distribution of EB-PVD coating

The difference in size between the evaporated surface of YPSZ ingot and coating area results in a non-uniform coating distribution. In order to accurately describe the effects of coating parameters, the differences between different parts of the samples and the difference in samples mounted to different fixtures must be established. To determine the coating

distribution pattern over the 410x150mm working area, the following distribution test was conducted on wire mesh made of AISI314 stainless steel (see Appendix A and Figure 24). The exemplary mesh (see Figure 24) was sandblasted, cleaned and coated during EB-PVD process (see Table 5 below for coating parameters).
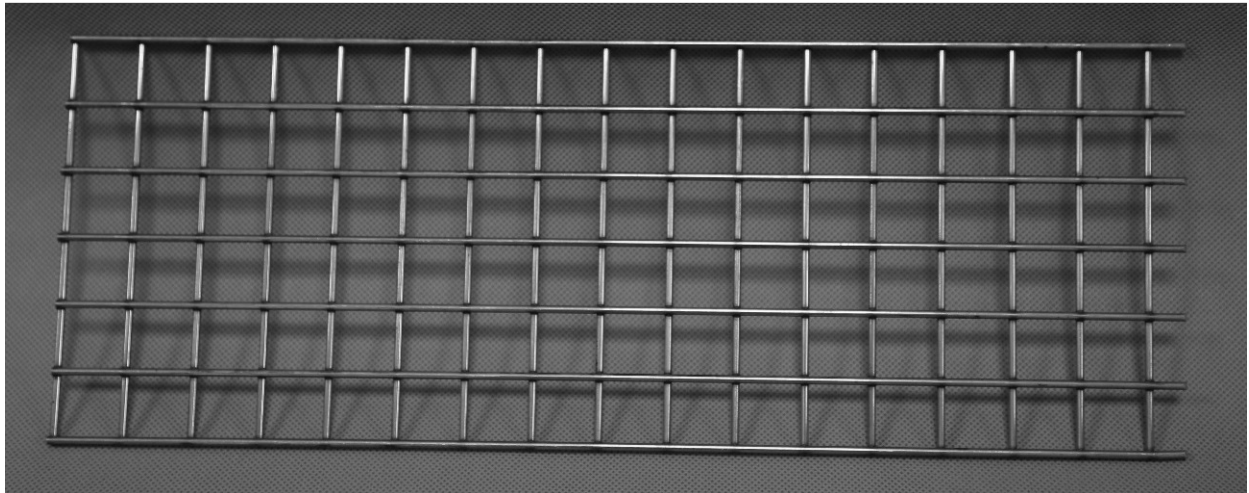
Figure 24. Wire mesh used for distribution test (photographed by M. Du Plessis, 2014).

Table 5: Parameters of EB-PVD process for deposition of ceramic coating on AISI314 wire mesh

Coating time	1200s
O_2/Argon flow ratio	90:10
Coating chamber pressure	0.01251 mbar
Emission current	2.77A
Ingot feed rate	1.6 mm/min
Ingot used	32.01 mm
Mesh weight gain	17.75 g
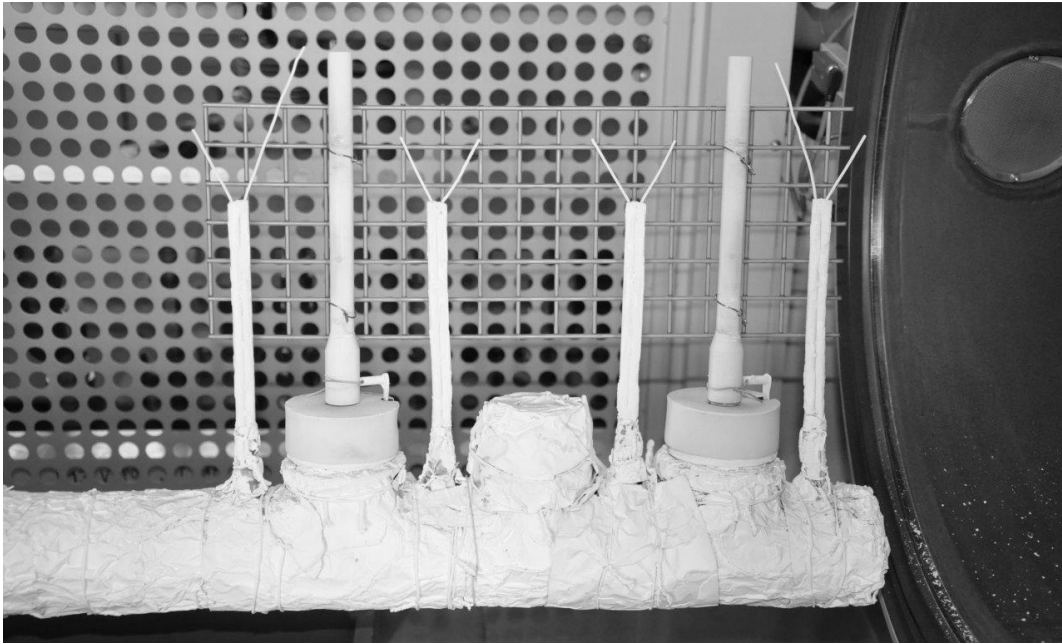
Figure 25 410x150 AISI314 mesh mounted to fixtures before coating process. The mesh will be cut into 102 nodes and coating thickness extrapolated to generate a distribution map (photographed by Slawomir Kotowski, 2014)

Afterwards, the mesh with one hundred and two points of interest (mesh nodes) was prepared for microscopic observations. After mounting in DuroFast™ resin, the mesh was cut into pieces, each with one point of interest. The effects of vibration on the mesh during cutting was minimized by using a Struers Accutom-50 cutting machine and CBN BOC13 cut-off wheel; these cutting conditions (the same as in Table 2) were found to produce minimal fracturing and burring on the edges of mesh. Samples were systematically mounted in Durofast™, and then polished using the polishing procedure discussed above (see section 6.3 polishing procedure) with the exception that samples were only polished to a SiC grit of 500, as the purpose of this analysis was to measure YPSZ coating thickness without the need for high column definition.

Coating distribution was measured using optical microscopy, perpendicular to mesh surface (i.e. surface facing ingot, found by measuring columns perpendicular to mesh substrate). The non-magnetic nature of AISI314 stainless steel made eddy current thickness measurements susceptible to error; however, the distribution profile could be confirmed using this method. It was established at several points spanning no more than a 20µm sector. The analysis from 102 samples produced the results shown in Figure 27.
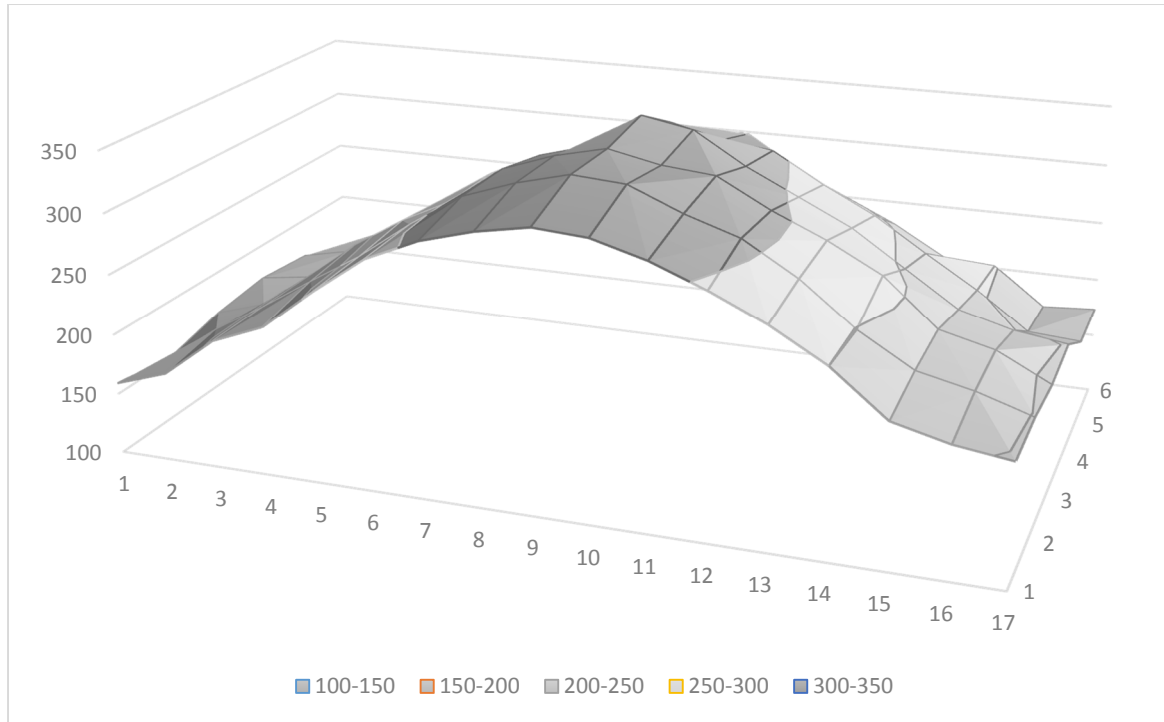
Figure 26. Exemplary distribution pattern showing thickness distribution diminished radially from point perpendicular to ingot centre. Y-axis and legend shows coating thickness in μm; X and Z axis are node coordinates.

The cosine model is valid for a small-area evaporator where the diameter of the melt pool is relatively small, compared to the distance between the melt pool and the substrate (see Figure 24).
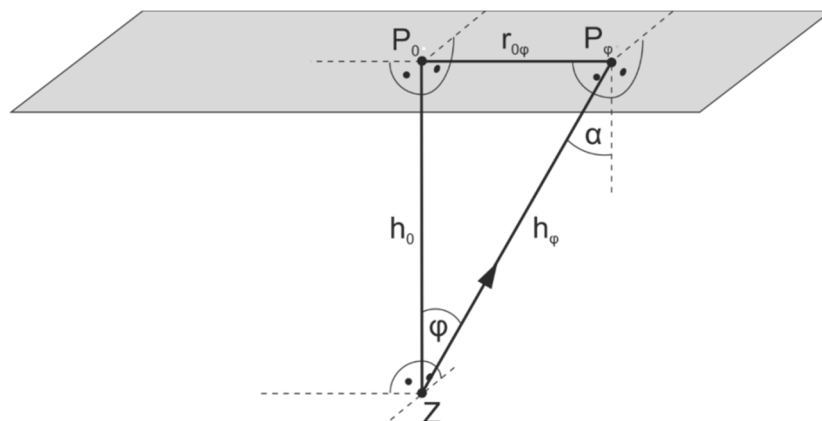

Figure 27. Graphical illustration of cosine rule for use in determining coating thickness at P_ϕ (S. Kotowski. 2014)

Table 6: Interpolated coating thickness at selected points of wire mesh

	Coating thickness (μm)	Average deposition rate (μm/s)	Intensity (ratio)
Max. thickness	334μm	0.29	1
Min. thickness	151	0.65	0.41
Left and right fixtures	248 μm	0.22	0.74

This allows for the explanation of coating thickness variance across the working area and confirm that this variance is within expected levels. The ceramic plume is not spherical and is under the influence of one or more of the following variables:

- Emission current of electron beam,
- O_2:Ar Gas flow ratio,
- Working pressure in the coating chamber,
- Electron beam aggressiveness, controlled by adjusting the beam focus and size scanning pattern on the ingot surface.
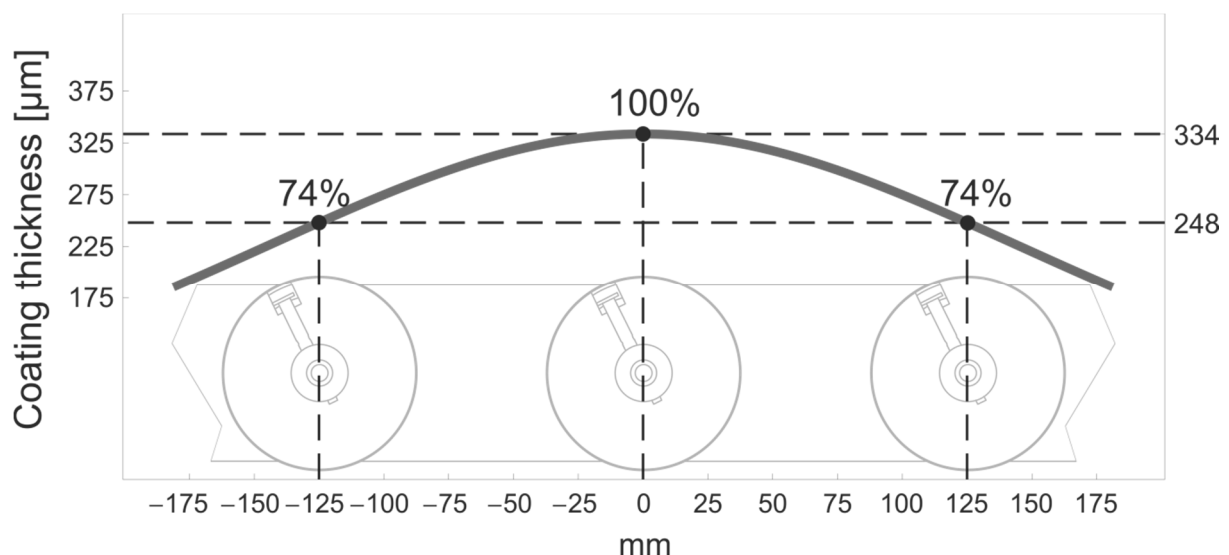
Figure 28. Graphical representation of coating distribution between central and side fixture (S. Kotowski. 2014).

Below is an exemplary thickness distribution obtained during a process characterised by high beam aggressiveness (Figure 29).
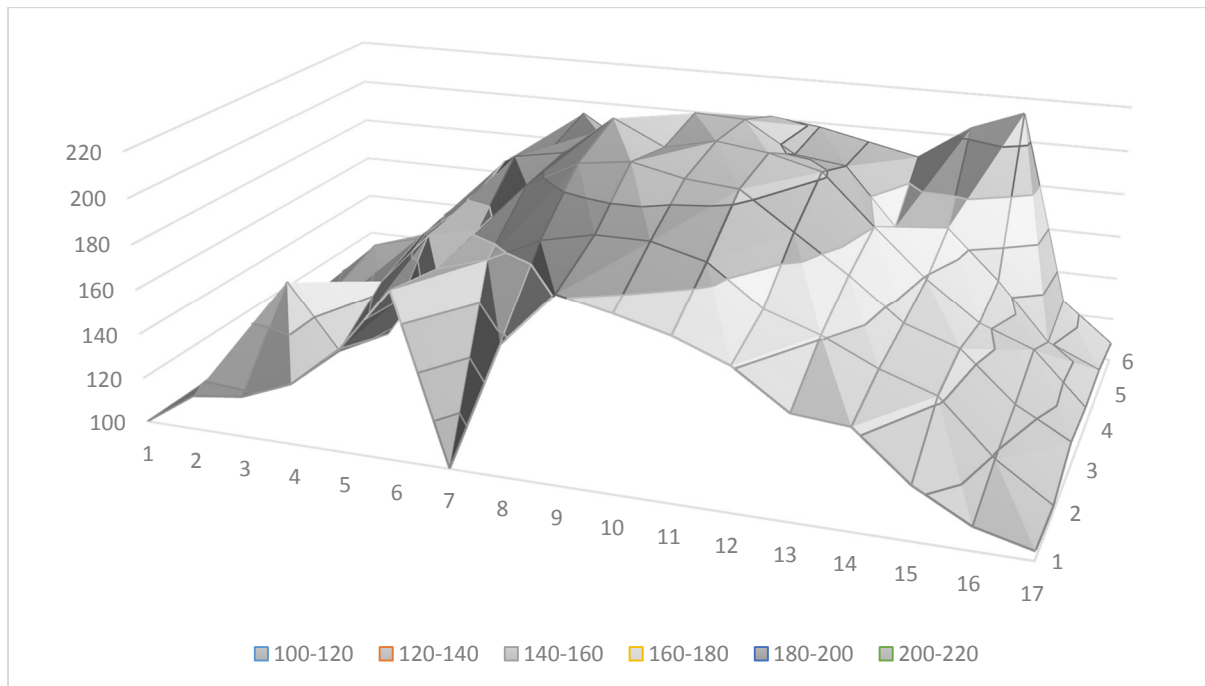
Figure 29. Irregular thickness distribution pattern obtained during EB-PVD process characterised by high beam aggressiveness, indicating that it may be outside the process window.

There is a significant variation in coating thickness between the centre fixture and side fixtures. This 26% difference will likely result in differences of morphology and ultimately in thermal mechanical properties. Comparison studies with flat samples resulted in a difference of 28% between centre and side fixtures. This suggests that the coating distribution pattern will only be mildly influenced by changes in input variables within a predefined operating window (discussed later) and also shows that impedance of the plume does not really influence the coating distribution pattern.

5.6 Operating window for EB-PVD coating

The relationship between Electron Beam Physical Vapour Deposition input parameters are important in the sense that coating distribution, surface morphology, thermal conductivity and YPSZ roughness are directly influenced by these variables. The output variable response surface is the subject of a study being carried out in parallel with this report, and will not be covered here. However, before the output variables can be predicted, an understanding of the relationships between input variables and their respective effects on the process environment is required. The number of input variables coupled with the uneven weighting of each variable lends itself to a non-linear model, the nature of this model is the objective of this section.
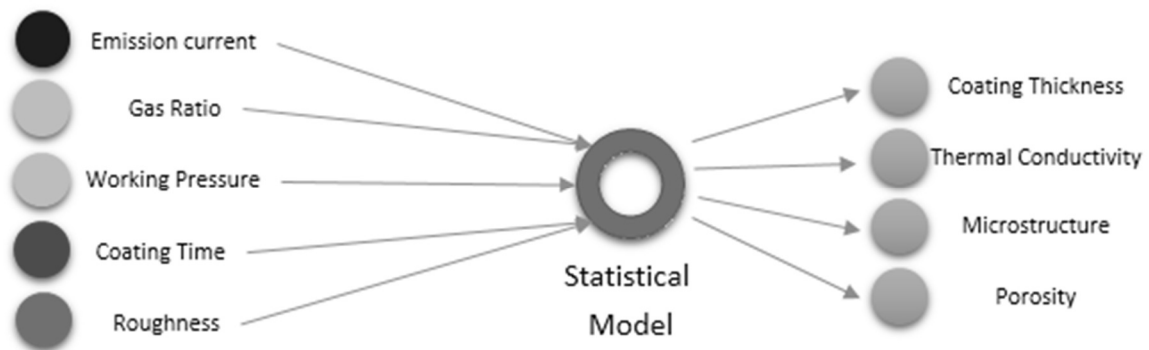
Figure 30. The input (left of model) and output variables (right of model) required to predict/analyse 10% YPSZ TBC coatings.

The goal of this section is to identify and asses the interactions of the input variables given above; this would ultimately add to the prediction accuracy of the output variable model. Thirty one individual experiments were conducted, in which input variables were modified to produce a range of coating environments between limits initially estimated. The experimental conditions were calculated by using Design-Expert© software (version 8.0.7.1). For a process to commence, a stable condition had to be achieved for a period of 3 minutes.

The definition of well-established coating conditions is given as follows (S. Kotowski. 2014):

1. Relatively flat, not "aggressive" surface of melted ceramic pool,
2. Stable values of pressure, emission current, process gas flows, temperature in coating chamber and gun chamber,
3. Adjusted evaporation rate to the ingot feed rate. The melted ceramic surface maintains the same height during the process.
4. No "spitting" effect. It can be caused by poorly adjusted (too high) beam aggressiveness. It can be observed visually during the evaporation. It results in transferring larger particles of ceramic material to the substrate surface, thus deteriorating the coating structure and quality.
5. No "build-ups" – ceramic material agglomerating around the melted ceramic pool. High "build-ups" can alter the plume geometry and can generate "spitting effect" when ablated material falls onto the melted ceramic pool.
6. No "outgassing" effect. This can be recognised when the actual pressure is relatively high compared to the set point value and working gas flows are on their minimum set

point values. It can be avoided by proper storage and preheating of ingot material and performing a suitable procedure for emission current ramp-up prior to the process.

7. No "arcing" effect. It occurs during poorly performed emission current ramp-up before the process ("outgasing") or if, after replacement, the new cathode and anode are not cleaned properly.

Figure 31 10% YPSZ ingot being melted by electron beam during the experiments discussed in this report (photographed by Slawomir Kotowski, 2014).

Response Surface Methodology (RSM) is a combination of mathematical and statistical techniques allowing the design of a model with many input variables to be calculated in fewer runs as compared to a similar factorial model (Sastry, 2012). By conducting the abovementioned processes and applying regression analysis, the output responses such as thermal profiles and ingot feed rate can be expressed in terms of input variables such as gas flow ratio, working pressure in the coating chamber, and emission current of the electron beam.

Identification of predominant factors which influence feed rate and thermal profile requires a mathematical model to be established in order to analyse these responses, in turn optimising the coating process. This problem is solved using a response surface D-type optimisation of a multi objective function model which identifies the primary factors affecting responses. This model is created using Design-Expert© software (version 8.0.7.1).

Utilising a polynomial surface reduces computational load (Boon, 2007); however, this means that gaps in the design matrix substantially alter the generated response surface due to experimental errors or sample contamination. However, there is a significant benefit in this approach. Despite the large number of input variables used, it was possible to obtain good results with far fewer runs than if a factorial analysis was performed. The aim of developing the mathematical models is to correlate the output responses with the input parameters, and thereby optimise the EB-PVD process.

The mathematical model is represented as:

$$Y_i = f(E, P, G),$$

where Y_i is the ith ingot feed rate (output variable), E is the emission current of the electron beam, P is the working pressure in the coating chamber, and G is the O_2:Ar gas flow ratio. The variation of input weighting suggested that the regression model linking the responses to the input variables would be a cubic polynomial function of the form:

$Y =$

$$\overbrace{b_0x_0 + b_1x_1 + b_2x_3 + b_3x_3 + b_{12}x_1x_2 + b_{13}x_1x_3 + b_{23}x_2x_3 + b_{11}x_1{}^2 + b_{22}x_2{}^2 + b_{33}x_3{}^2}^{\text{quadratic model}}$$
$$+\ b_{123}x_1x_2x_3 + b_{112}x_1{}^2x_2 + b_{112}x_3{}^2x_3 + b_{122}x_1x_2{}^2 + b_{133}x_1x_3{}^2 + b_{223}x_2{}^2x_3$$
$$+\ b_{233}x_2x_3{}^2 + b_{111}x_1{}^3 + b_{222}x_2{}^3 + b_{333}x_3{}^3$$

Y is the third order output response, x_1, x_2, x_3 are the input parameters, namely the emission current, the working pressure and the gas flow ratio. b_1, b_{12}, b_{123} are estimates based on least squares. The function in terms of feed rate is given later on.

However, this was disproved in subsequent experiments and, eventually, a linear model was used for some of the ANOVA tests, which is discussed further in the text. Experiments were conducted using the maximum and minimum values. These values were altered during experimental setup. Arcing, poor melting and beam instability were the signalling factors for the process boundaries to change. The variables were all categorised as numeric factors. Emission current and O_2:Ar gas flow ratio were discretised, while vacuum pressure was considered to be numeric.

Table 7. Input parameters for distribution test

Emission Current	Pressure	Oxygen
A	Percentage	mbar
Discrete	Discrete	Continuous
11	7	N/A
2.3	20	0.008
2.4	30	0.016
2.5	40	
2.6	50	
2.7	60	
2.8	70	
2.9	90	
3		
3.1		
3.2		
3.3		

The twenty-one-run design matrix consists of thirteen runs, five lack of fit runs and three replicates. The responses are listed below. Data from eight thermocouples mounted on a feeder made it possible to establish the thermal profile during the coating processes (see Figure 43). Temperatures, beam focus (Focus 1 and 2), pattern zoom (Zoom X and Y) and offset (Offset X and Y) represent the parameters of the EB-PVD process at the respective inputs. The responses are given below:

Table 8. Responses measured using regression analysis.

Blade thermocouple 1	°C
Blade thermocouple 2	°C
Blade thermocouple 3	°C
Blade thermocouple 4	°C
Blade thermocouple 5	°C
Blade thermocouple 6	°C
Rake thermocouple 1	°C
Rake thermocouple 2	°C
Focus 1	A
Focus 2	A
Zoom X	A
Zoom Y	A
Shift X	A
Shift Y	A
Ingot feed rate	mm/min

Analysis of Variance (ANOVA) was utilised to quantify the significance of the developed statistical model. The correlation values for quadratic and cubic models were 0.862 and 0.929 respectively, appearing at first to confirm the assumption about using a cubic model made at the beginning of the experiments. However, predicted correlation values for the cubic model was -30.4. This is exceptionally large when compared with the closest value which was for the quadratic model at 0.515. Furthermore, the PRESS (predicted residual sum of squares) value for the cubic model was 8.56 as opposed to 0.13 for the quadratic model, indicating a significant lack of fit in the cubic model. The decision to revert to a quadratic model was based on these findings, and the fact that future refinement of the model could be made to improve the R value of the quadratic model, while improving the lack of fit to an acceptable value would require significantly more runs. The P value for the quadratic model is less than 0.05 indicating model significance.
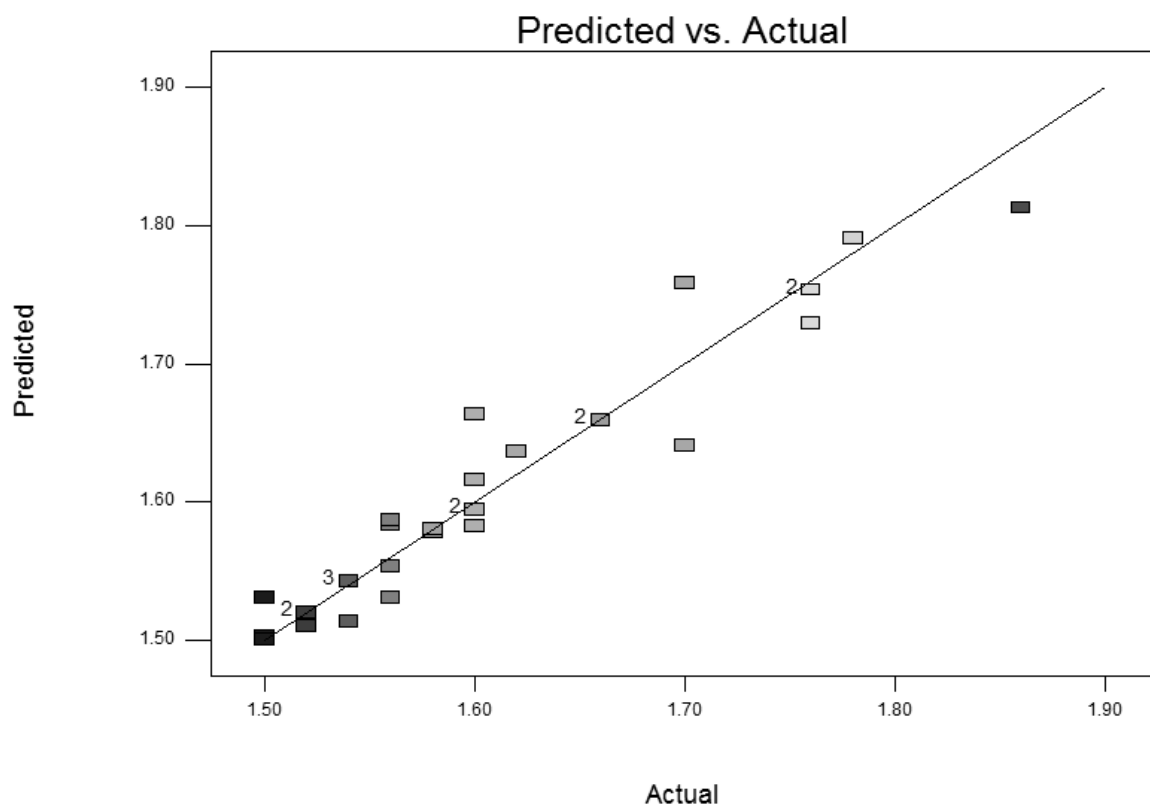
Figure 32. Current Prediction versus Actual Feed Rate chart, graphically representing the R value of the quadratic model, each individually coloured point signifies an individual run (M. Du Plessis. 2014).

The empirical model for output response (ingot feed rate) in terms of listed input variables was developed by using the RSM method and was further used for optimisation of the coating process. The regression coefficients were determined through regression analysis, and quadratic models were developed due to the lower predictability of the third order (cubic)

responses. The following equation was obtained in terms of actual factors individually for feed rate.

$Ingot\ feed\ rate$

$$= 1.87 - 0.584 \cdot E + 78.86 \cdot P - 3.65 \cdot G - 8.9 \cdot E \cdot P - 0.000476 \cdot E \cdot G - 0.211$$
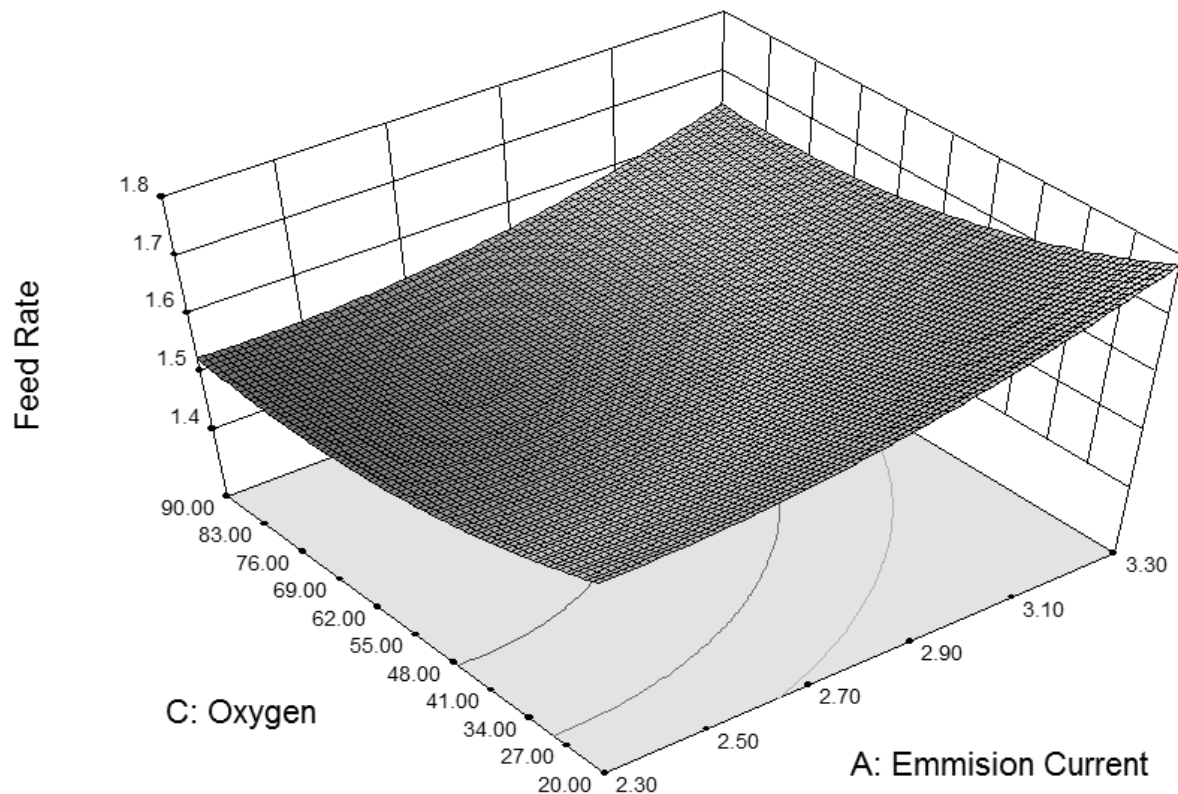$$\cdot P \cdot G + 0.152 \cdot E^2 - 1872 \cdot P^2 + 0.541 \cdot 10^{-5} \cdot G^2$$

Figure 33. 3D surface depicting Feed Rate at 0.012mbar. Any condition within the process parameter window can be simulated once the model has been established and used to predict process parameters.

Optimisation of the response surface is carried out within Design-Expert© software, with the goal of verifying the model. Several parameters were selected (temperature, feed rate, working pressure, etc) and the experiement re-run with the given goal, i.e. confirmation of responses input to determine the model realiability. Ten Points were chosen and used for optimisation. The final conformity value was 0.932; considering the correlation value, this is a satisfacotry result. The model can thus be considered reliable; however, this is still subject to further verification.

Observations made during the experiment can be described in terms of the primary input variables - temperatures, ingot feed rate and working pressure. The temperature profile across the coating area is not linear; however, the effects of input variables on each thermal zone follows the same trend throughout the expriments.
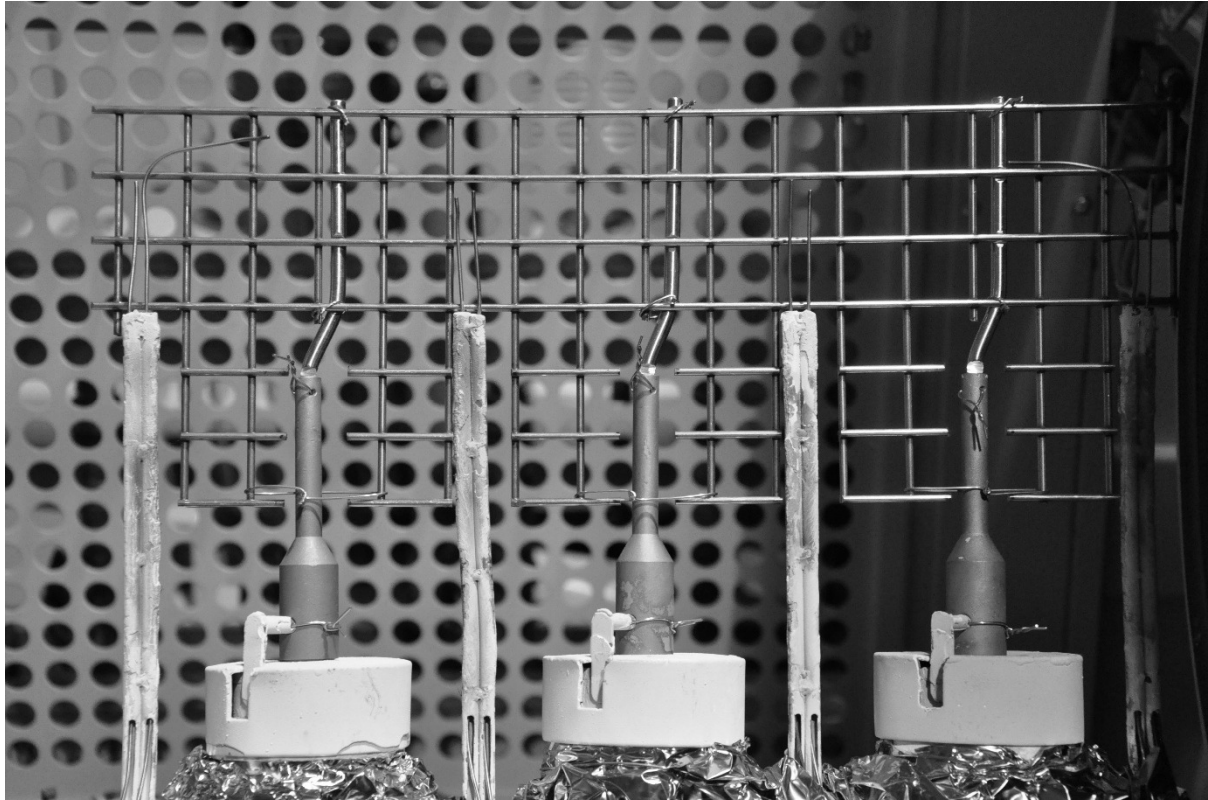
Figure 34. Thermocouples within the coating area, used to show the thermal profile across the coating area (Research and Development Laboratory for Aerospace Materials, photographed by M. Du Plessis, 2014).

The temperature profile is significantly influenced by emmission current. A maximum change of 113.2 °C is observed in the thermal profile from minimum to maximum emmision value as apposed to the 23.6 °C observed across working pressure extremes and 28.9 °C across O_2:Ar flow ratio extremes. These values are based on a linear model shown in Figure 35 below.

Table 9: Percentage influence of selected input variables of EB-PD process on temperature distribution, assuming linear perturbation.

Thermal influence (%)	
Emission current	*68.32*
Working pressure	*14.24*
O_2:Ar flow ratio	*17.44*
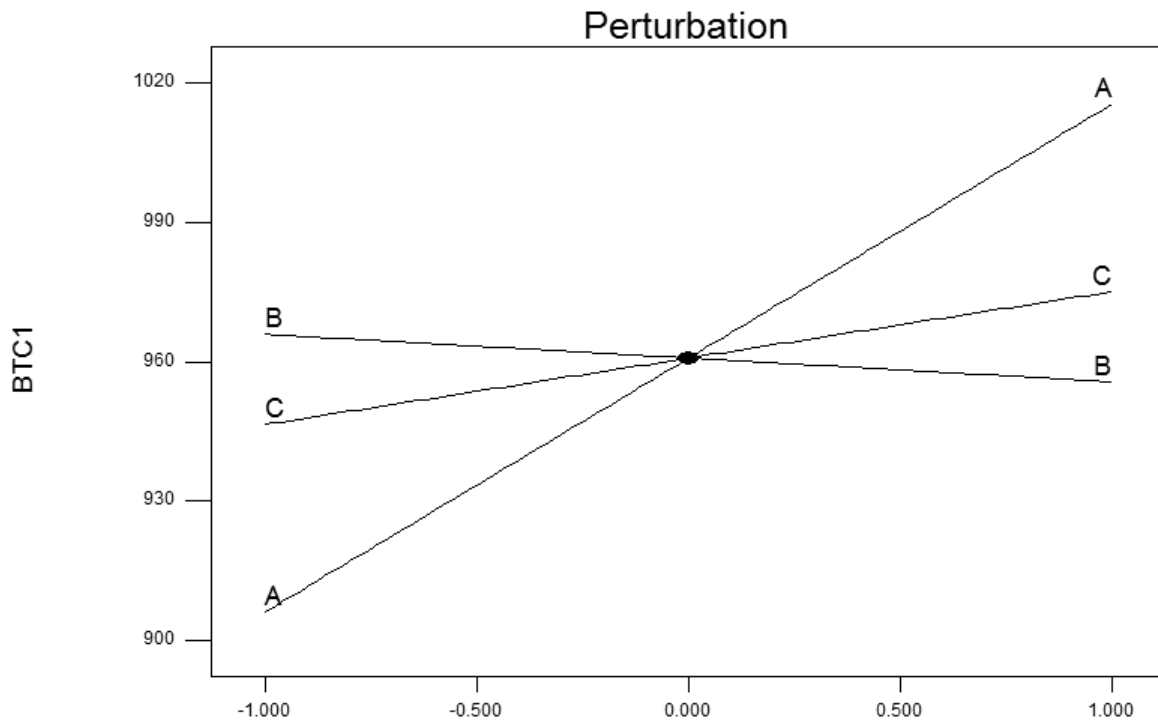
Figure 35. Perturbation graph showing interaction of input variables at central point in design matrix. Created using Design-Expert© software (version 8.0.7.1). Emission current (A), control pressure (B) and gas ratio (C).

The quadratic model for ingot feed rate depicts two significant input variables: emission current and O_2:Ar gas flow ratio. Emission current (A) causes an increase of ingot feed rate. This is expected as the temperature of the melted ceramic pool increases with aggressivity of the electron beam. The reduction of feed rate with an increase in O_2 flow (C) content may be attributed to the role of O_2 in the process, discussed later on. The working pressure in the coating chamber (B) appears to have a negligible effect. However, the effect of coating pressure on morphology, specifically column porosity, is important. This is the subject of a concurrent study outside the scope of this thesis.
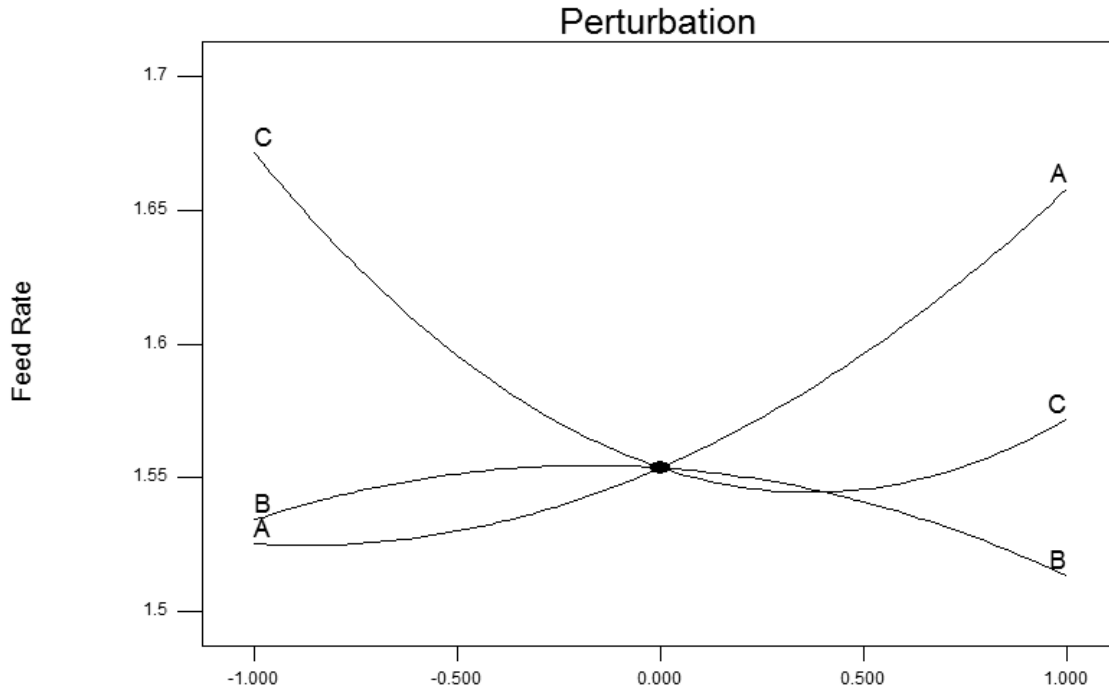
Figure 36. Perturbation graph illustrating the significance of emission current (A) and gas ratio (C). Pressure (B) has little effect on feedrate; however the effect on morphology is yet to be investigated.
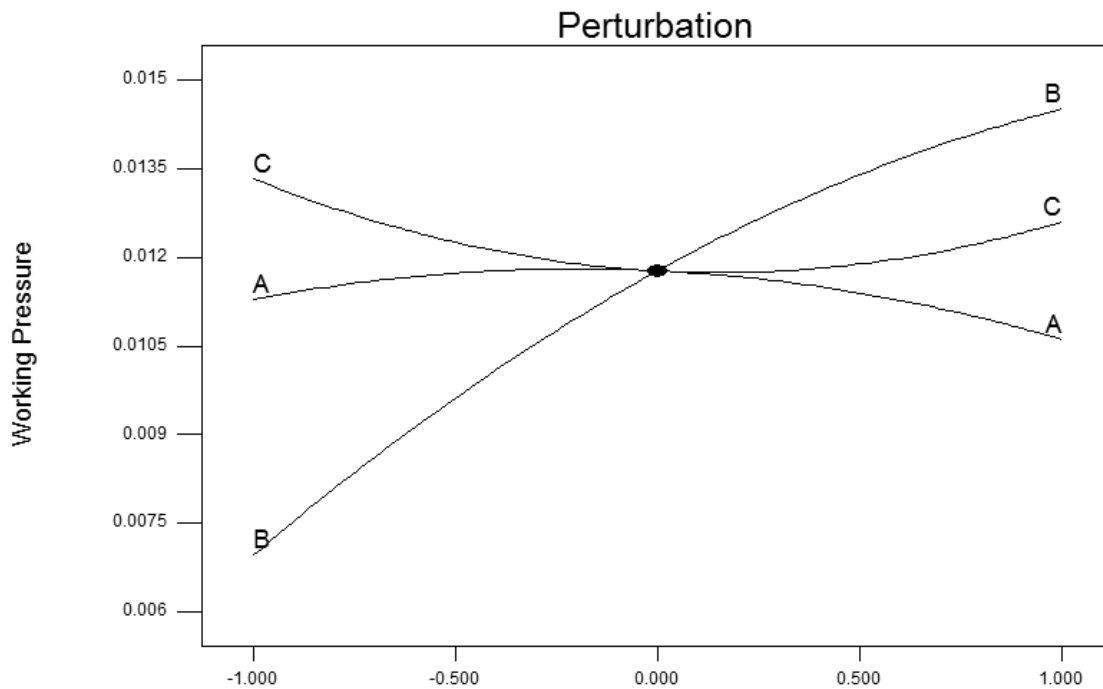

Figure 37. Effects of input variables on working pressure. Emission current (A), control pressure (B) and gas ratio (C).

Feedrate can be described as the primary factor concerning the coating process. This view neglects the response effects on coating morphology. Optimisation runs were undertaken for

maximum, minimum and central feedrates. Optimisation runs each have multiple iterations of input variables; the best combination is determined by the required morphology. The following results were observed.

Table 10: Input values from feedrate responses

Feed Rate Response			
	Pressure	Gas Ratio	Emission Current
Minimum	0.008	15:09	2.34
Central	0.009	07:20	3.12
Maximum	0.012	01:04	3.30

5.7 Deposition and analysis of CVD-NiAl/EB-PVD-YPSZ TBC coating

40x30x5mm Inconel 617 samples were machined from sheets. Matching sample holders were designed and manufactured (See Appendices D). The large size and rectangular shape of the samples made polishing with the TegraPol 25 impossible. Instead, a rotational polishing method was used (See Figure 38). Samples were machined at different rates for various periods of time, before the CVD process commenced. This was carried out to confirm the Influence of substrate roughness on CVD roughness, discussed earlier. Final substrate roughness varied between 1.7µm and 0.4µm. An aggressive polishing method (See chapter 5.3) was used, rounding off of edges was found to be minor. This would have no bearing on the final results as measurements were not considered at the edges.
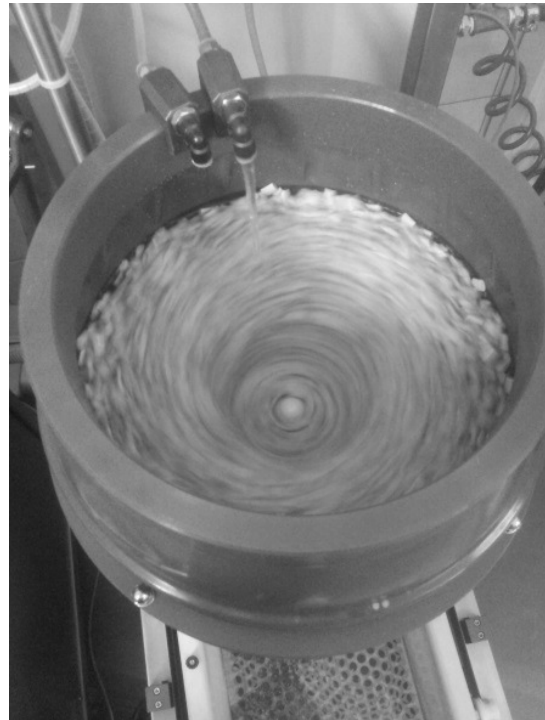
Figure 38(a). Avalon TE-18 centrifugal tumbler and (b) process chamber during polishing of Inconel617 sheets.

Figure 39. Inconel 617 samples being loaded into CVD process chamber for coating (photographed by Slawomir Kotowski, 2014).

Initial setup of the following model followed much the same route as "coating distribution" above with the exception that different variables were examined (see Figure 30). The final analysis is a culmination of all the work above in which samples were coated in the ALD smart coater™ and analysed via optical microscopy to establish a response surface for the following coating properties, coating thickness, coating density and quality of coating.
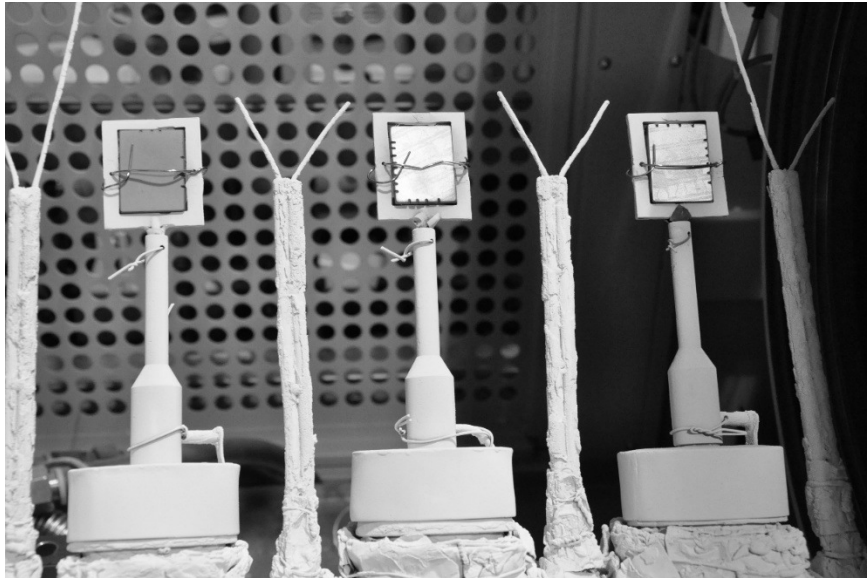
Figure 40 Samples being prepared for coating, each sample has a different Surface roughness as this is the only variable distinguishing each of the 3 samples coated per processes (Research and Development Laboratory for Aerospace Materials, photographed by M. Du Plessis, 2014)
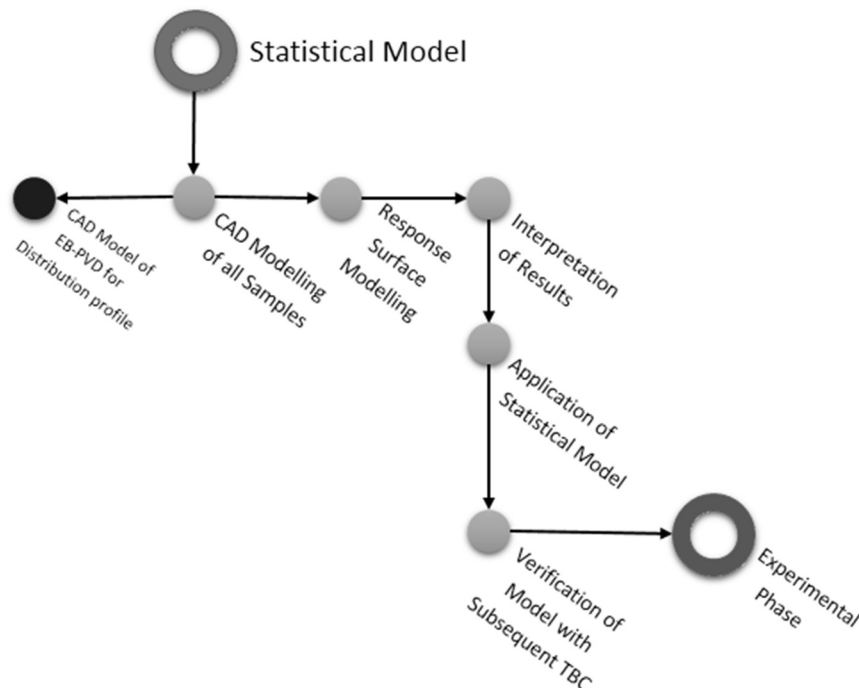
Figure 41 Process followed during creation of the statistical model

The boundaries for process parameters were chosen within the EB-PVD process window discussed above, in order to maintain stability and avoid being susceptible to errors which occur at the process fringes (see Figure 29). Values used during the process were:

Table 11 Higher and lower limit values of parameters used for Response Surface Method.

RSM boundary values			
	Emission current (A)	Working pressure (mbar)	Gas flow ratio (O_2:Ar)
min.	2.4	0.008	30:70
max.	2.8	0.012	70:30

The role of temperature also needed to be understood. Temperature is a dependent variable influencing each output differently. The correlation between temperature and emission are investigated below. The thermocouple provides only ambient temperature around the sample, however the significance of this temperature difference needed to be investigated. The author made the following assumptions:

- The average temperature between thermocouples Blade 1 and Rake 1 represents the ambient temperature of the sample between these thermocouples, the other fixtures follow the same logic.
- Conduction between sample and fixture holder would be ignored as this zone is less dynamic than the rest of the sample surface.
- A low heat flux would be used when considering losses, due to the high vacuum pressure in which the process is conducted.
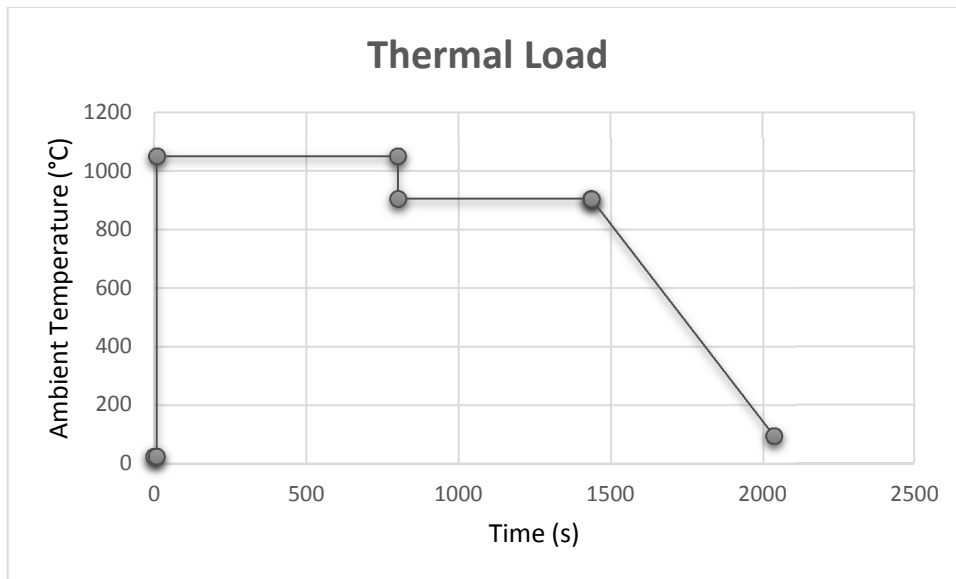
Figure 42 Thermal loading condition applied to ambient conditions around sample during one of the experimental processes and similarly to the simulation below
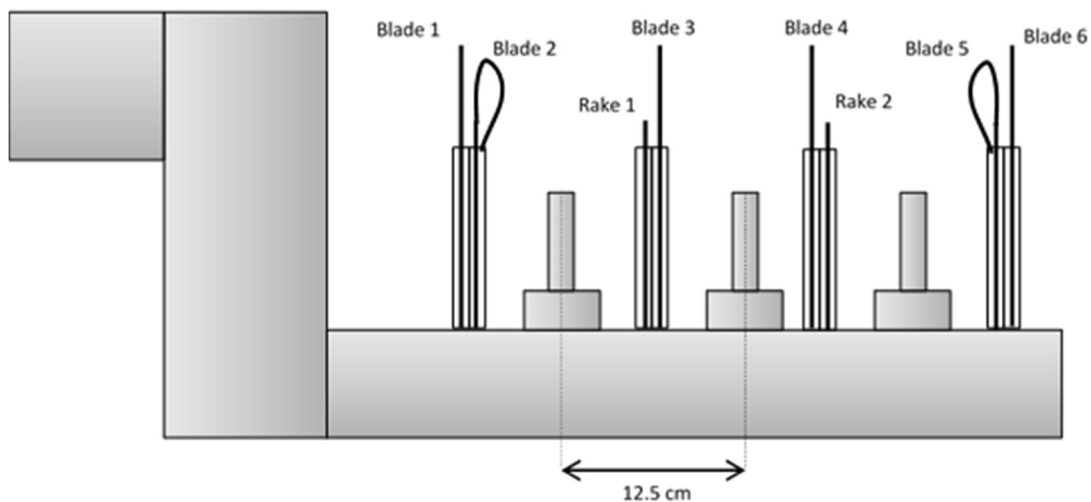

Figure 43 Thermocouple locations relative to fixtures, used to calculate ambient temperature around the sample, a result of the electron plume (S. Kotowski. 2014).

Abaqus™ Simulia package was used for the following transient heat simulation, performed over the entire duration of process, the time of highest temperature in the coating chamber (i.e. between 800 and 1435 seconds) would be taken into account in the statistical model and carried over to all samples within the same coating duration, identical simulations would be done for the 415 second and 525 second samples also. The Model used represents the samples used in the coating process. All material properties are specified for Inconel 617.

Simulation results were taken at 810 seconds just as the sample left the heating chamber and entered the coating chamber. At this point temperature difference between sample and thermocouples is greatest added to the fact that this is the period when surface temperature has the most significant as the top-coat has direct contact with the sample. Results showed the following differences temperature.

Table 12 Average values calculated from simulation to be added to sample temperature results in statistical model.

	635 second process
Temp. difference at 810 sec	*85.9℃.*
Temp. difference at 1435 sec	*4℃.*
Average sample difference ($Δ_{av}$)	*21.5℃.*

$$T_{left\_sample} = \left(\frac{T_{blade2} + T_{rake1}}{2}\right) + Δ_{av},$$

T_{Left_sample} denotes the temperature in the area of specific fixture T_{blade} and $T_{rake\#}$ indicate the adjacent thermocouples. $Δ_{ave}$ refers to the change in average surface temperature between sample and ambient temperature.
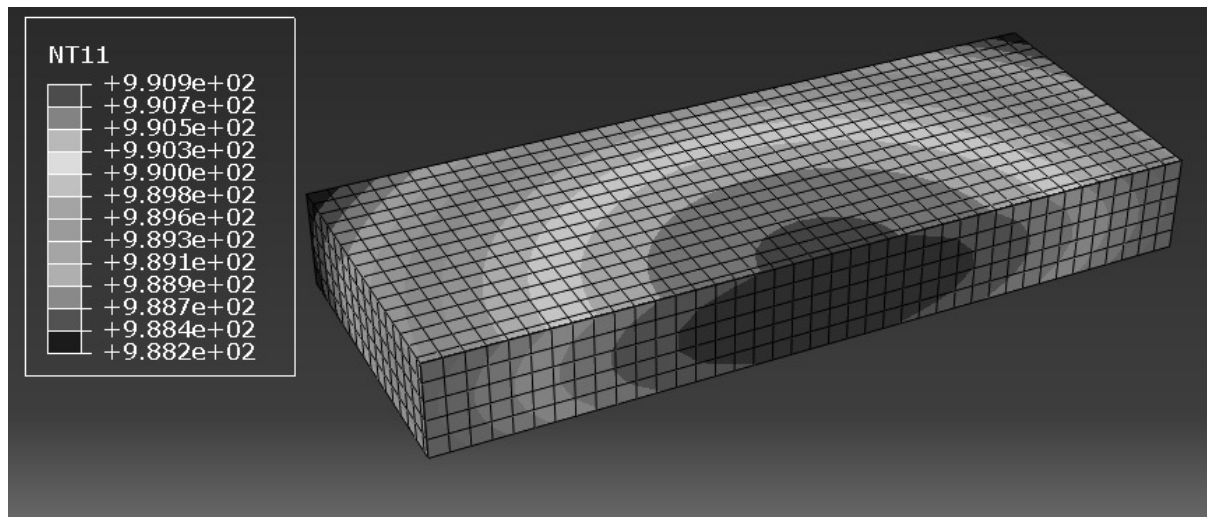
Figure 44 Abaqus™ simulation result for heat loss from the sample 10 seconds after leaving the heating chamber and coating begins.
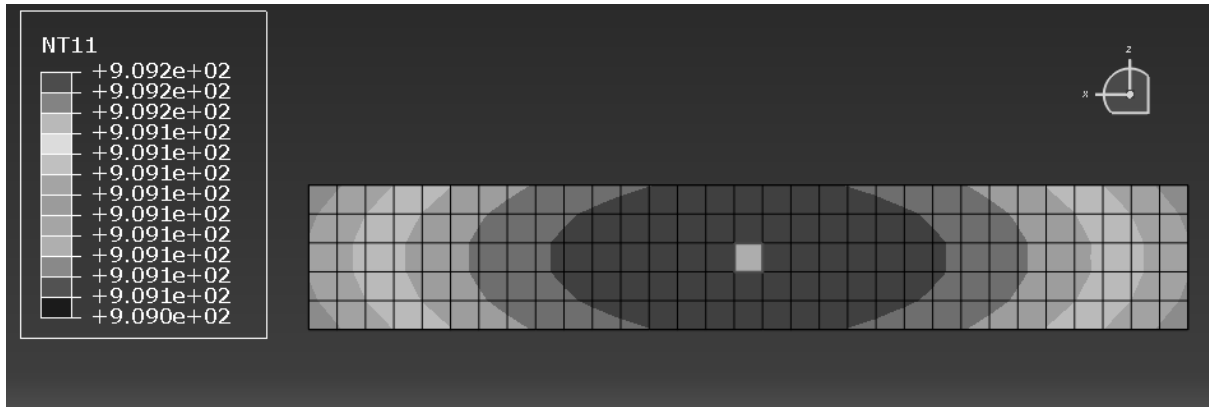
Figure 45 Cross-section of the sample at 1435 seconds.

Using the simulation results to compare change of distribution coefficient on central and side samples due by both emission and temperature shows a near linear relationship, proving that temperature is directly proportional to emission current between 2.4-2.8 Amps. This relationship bears further investigation at higher emission currents but for the purpose of this report it will be assumed that emission effect on output variables adequately represents the effect of temperature on those same variables.
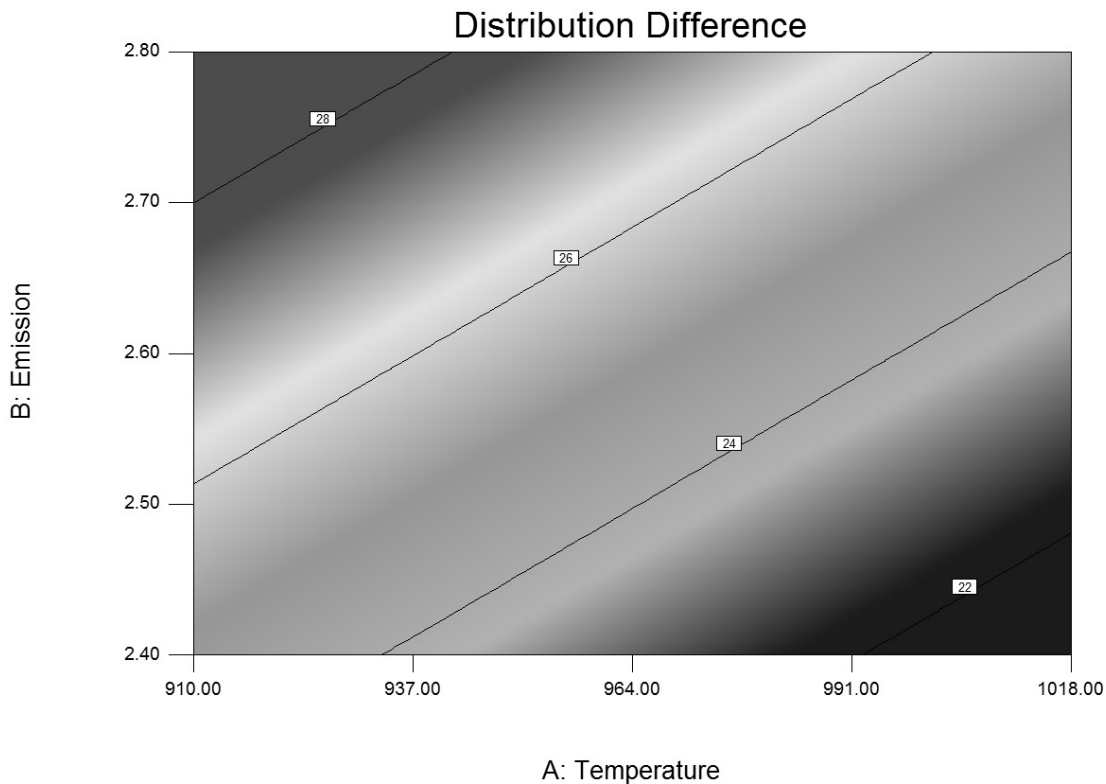
Figure 46 Thermal contour map showing deviation in distribution between central and side samples during coating process, proving the direct proportionality between emission current and temperature for coatings below 2.8Amps.

Design Expert™ RSM modelling for D-optimal conditions was used for design of experiment (DOE), regression modelling in order to estimate the significance of each of the inputs on output variables. The model consisted of input variables (See Table 11) and the following output variables:

- coating thickness
- upper Colum Density
- distribution Coefficient

Coating thickness refers to the thickness of only the top-coat from bond-coat to the outer column points. Made up of an average value taken at six random points along the substrate. Points were randomly selected however discounted if they fell above a defect or were themselves defective.
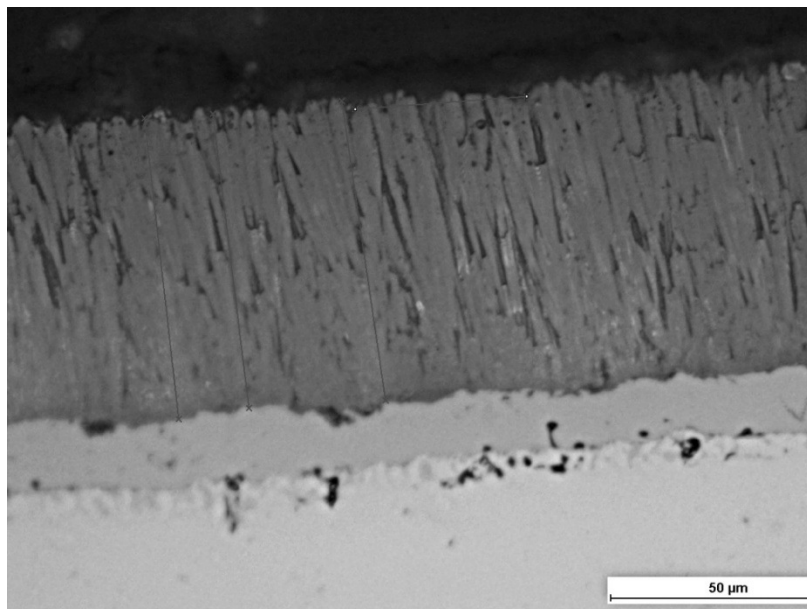
Figure 47 Picture taken on optical light microscope showing measurement lines. Vertical line on right is discounted.

Column Density was measured by counting the number of columns parallel to the bond-coat over a 50μm span. Column density represents a preliminary indication of relationship between column morphology and input conditions; however, more detailed research is required before this relationship may be quantitatively described.
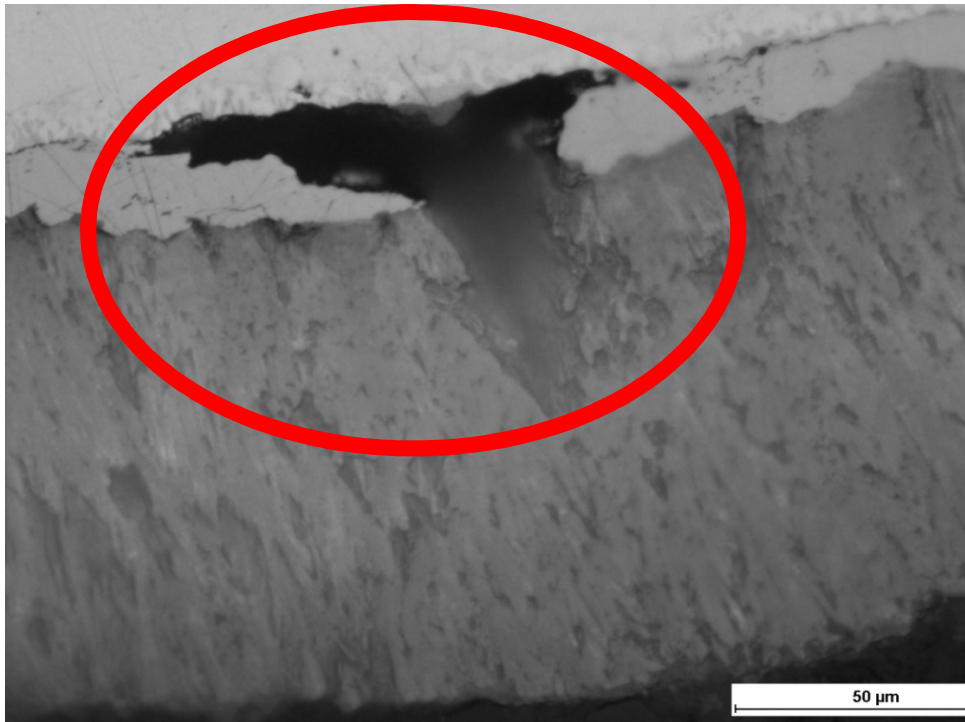
Figure 48 The micrograph shows a defect in the bond coat which may lead to coating failure through thermal loading. The statistical model is the first step in identifying causes of defects in TBC's.

A distribution coefficient is determined for each of the processes, this difference in coating thickness is a function of the sample coordinates within the coating area, temperature, electron bean emission current and bond-coat roughness. These results build on the initial result obtained during the "coating distribution" experiments discussed earlier.

The following regression model shows the relation between all input variables on the coating thickness. A linear model was chosen due to the exceptional Pearson product moment correlation coefficient obtained (R value) of 0.9957 (See Figure 49), indicating excellent correlation within the model for future prediction. The F value for this model was 12.97 indicating excellent prediction ability for future coatings.
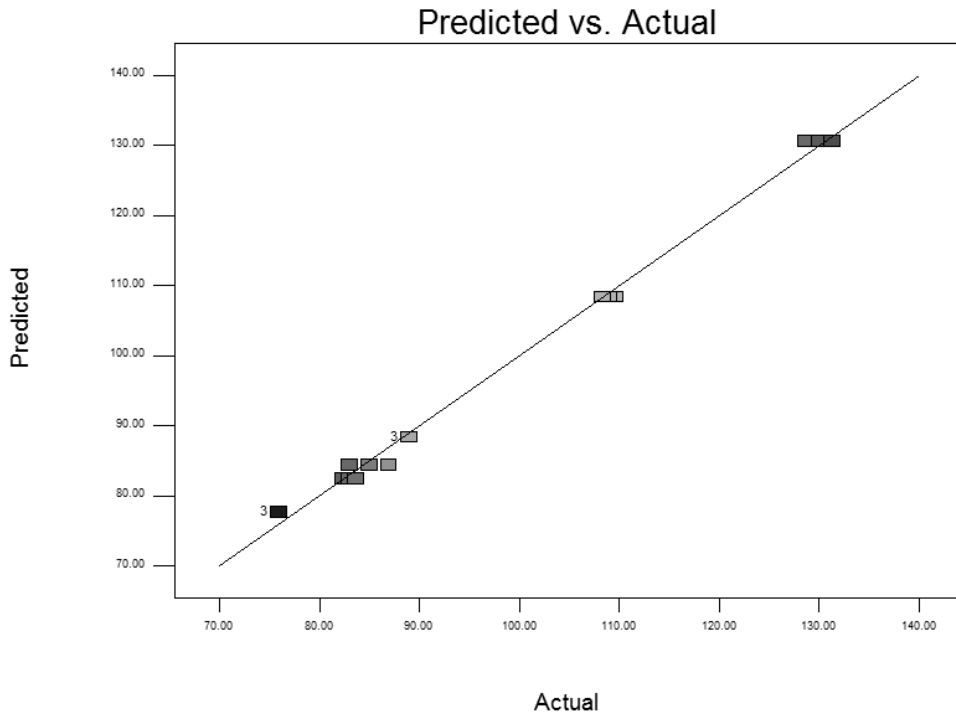
Figure 49 Graphical comparison of p value for coating thickness, illustrating the excellent results for this model.
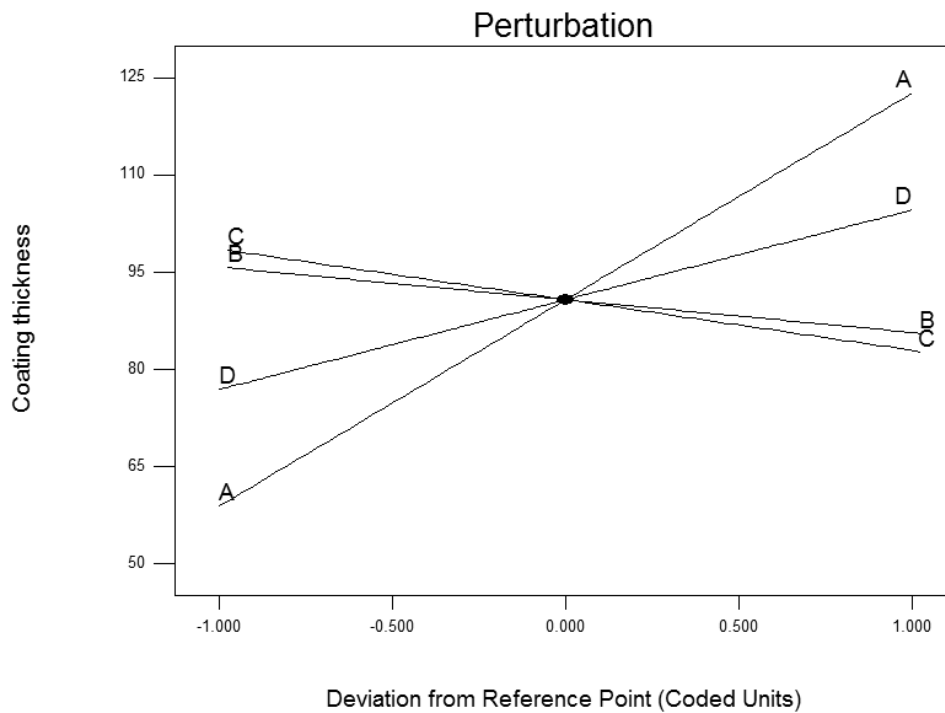

Figure 50 Input significance to model depicting, Coating time (A), oxygen content (B), emission current (C) and working pressure (D).

Coating time had the most significant effect on coating thickness, this follows logic and is confirmed in the distribution test results performed earlier. Working pressure significance was predicted in the EB window experiment covered earlier (See Figure 36 the rise in feed rate due to working pressure confirms this result), where an increase in pressure up to 0.012mbar had a positive effect on the feed rate, beyond this feed rate dropped. Emission current and oxygen had insignificant effects on the thickness, this however does not speak to coating morphology. The drop in thickness due to emission current is likely due to the narrow feed rate generated by the emission range of 2.4-2.8 Amps. This decrease in thickness with higher emission rates should not be viewed as a rule for EB-PVD, however a more significant emission parameter should be investigated in future experiments. The effect of Oxygen on the coating thickness follows expectations as O_2 only creates the environment for the electron beam to be produced while argon is the ionizing carrier for YPSZ.

Column density described by the amount of columns per μm on the outer edge of the top-coat was measure to establish a baseline for future morphology experiments (See Figure 51). Overall conclusions will be discussed further on.
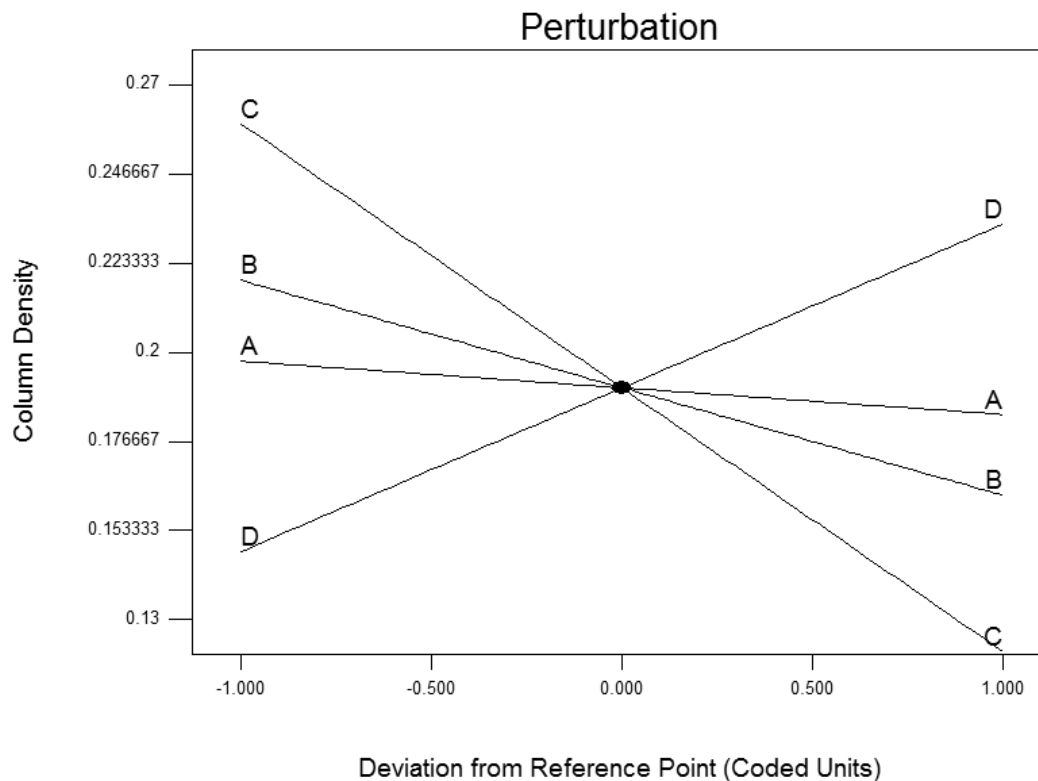

Figure 51 Column density Input significance, Coating time (A), oxygen content (B), emission current (C) and working pressure (D).

Experiments were successful in establishing variable significance in EB-PVD coatings. However more work is required to effectively quantify column morphology. This is due to large standard deviation in the model; this may be solved by conducting more experiments with the same methodology. The coating thickness model; however, produced excellent results for accuracy and prediction. Here it was able to establish a quantitative model for this parameter. Using a linear RSM model the following formula for thickness was generated:

$$Coating\ Thickness\ (\mu m) = -16.74 + 0.29 \cdot A + 0.25 \cdot B - 39.05 \cdot C + 6928 \cdot D,$$

where:

      A - coating time (s)

      B - oxygen flow content (%)

      C - emission current of electron beam (A)

      D - working pressure in coating chamber (mbar)

6 - Discussion

This dissertation attempted to illustrate and quantify the effects of input variables EB-PVD YPSZ top-coats in order to better explain variance in resultant TBC properties. In addition to the statistical models developed, sample preparation was investigated and documented as this proved to have direct bearing on inaccuracies transferred to the final results.

YPSZ thermal barrier coatings are susceptible to fracturing caused during sectioning, which is a required step for microscopic investigation? The effects of vibration and excessive polishing forces were show in Figure 16. A successful polishing procedure was established and the process together with comparative evidence of the difference between a "good" and "bad" process.

The relationship between substrate surface roughness and bond-coat roughness was considered. The effects of post processing of bond-coats on the top-coat is significant whereas it was shown that substrate roughness between 2µm - 18µm had a negligible effect on bond-coat Ra value. It may be concluded that less time should be spent on controlling substrate roughness and more time devoted to bond-coat roughness. The advantage of this is that it take substantially longer to alter an Inconel 617 substrate roughness by 2µm than to create the same change in a NiAl bond-coat. This is due to the hardness difference between these two materials. However the disadvantage to this is that uniform polishing of bond-coat is less likely when using blasting techniques which is currently the industry standard method for blade refurbishment.

Distribution was investigated and a distribution map generated for two coating experiments on either end of the coating window. Results showed the expected differences across the coating area and also illustrated the difference in uniformity between high and low emission beam aggressivity. A comprehensive analysis of the distribution mesh in future will further increase the resolution of the distribution variance for different input results. From the results it is clear however that there is a difference between central and side substrate fixture coating thickness, using cosine law however this difference can be predicted. The impact of sample geometry on the evaporative plume was shown to be insignificant contrary to initial assumptions made by the author. Variance during the more aggressive experiment (See Chapter 5.6 for upper and lower limits) was significant as shown in Figure 29. However further analysis done during the final statistical model showed that distribution variance within the narrow operating window of the model was only slightly influenced by changing input variables.

The coating window was established during a series of experiments in which a response surface was created using RSM with a quadratic D-optimal model. The results indicated that emission current and gas ratio were the most influential input variables, the effect of pressure however will effect morphology which will have to be further investigated in the future. Feed rate, working pressure and temperature at the substrate were the primary responses, the influence on these responses was discussed. Emission current and gas ratio have the most impact on the coating. From the results, the feed rate can be predicted and hence thickness controlled. Coating parameters obtained from the operating window model were used as process prediction values during the final processes, these predicted values (See Table 8) proved to be very accurate in setting up stable conditions, validating the operating window model.

7 - Conclusions

This dissertation set out to establish relationships between various input and output variables responsible for controlling the properties of EB-PVD top-coats. The experiments surrounding the creation of this model were explained and the final response surface created using the experimental results.

Two key points that were focussed on were column density and coating thickness. Regression modelling was successful in establishing degrees of sensitivity for each of these outputs and showed that each held different significance for the various outputs. The input variables and their roles were identified and discussed. In addition to the sensitivity analysis, the correlation coefficient and F-test for lack-of-fit obtained for coating thickness allowed a formula to be extracted. Verification of this formula showed a 93.5% accuracy when predicting coating thickness within the 2.4-2.8 Amp emission current range. Further verification is required to improve and validate this formula.

With regards to the input variables, emission current played the biggest role column density, possibly due to its effect on beam aggressiveness hence the increase in coating defects was not surprising. However the lack of significance on coating thickness suggests that a higher current limit be set for future experiments. Comparisons drawn with the operating window model suggest that the increase of coating thickness with regards to emission current is exponential (See Figure 36) and may explain this insignificance below 2.8 Amps. In addition to the above, it was shown that for the considered process window (2.4-2.8 Amps) emission current adequately represented temperature effect on output variables, making an additional temperature variable redundant in the model. Coating time had significant impact on coating

thickness and mild impact on column density. Thicker coatings allow more column growth and hence "column selection" reduces the number of columns seen at the surface of the top-coat. This leads to the higher roughness averages suggesting that CVD roughness only plays a role in mechanical failure at the TGO layer during thermal cycling and does not have significant bearing on the final morphology of the top-coat. A full morphological analysis is necessary to determine the validity of this claim. Oxygen to argon ratio had less effect than the other input variables. However, similar to working pressure, the effect on morphology requires more research.

Statistical analysis is an ongoing process, data mining from experimentation on the SMART Coater™ will be ongoing, constantly adding to the model and improving its accuracy. The initial results shown in this dissertation prove that despite the massive amount of variables involved in the EB-PVD coating process, the outputs can be successfully quantified and predicted assuming that the prediction model has enough data.

Bibliography

Airbus. (2014, March 15). *Airbus*. Retrieved from Passenger Aircraft: http://www.airbus.com/aircraftfamilies/passengeraircraft/a380family/

Anon. (2012, December 23). *Standard_deviation*. Retrieved from Wikipedia: http://en.wikipedia.org/wiki/Standard_deviation

Avallone, E. A., Baumeister, T., & Sadegh, A. (2007). *Marks' Standard Handbook for Mechanical Engineers Eleventh Edition.* New York: McGraw-Hill.

AVALLONE, E. A., BAUMEISTER, T., & SADEGH, A. (2007). *Marks' Standard Handbook for Mechanical Engineers Eleventh Edition.* New York: McGraw-Hill.

Berger, R., & Casella, G. (2001). *Statistical Inference, Second Edition.* Cengage Learning.

Boon, J. (2007). Generating Exact D-Optimal Designs for Polynomial Models. *National Security Technology Department Journal*.

Choy, K. (2000). Chemical vapour deposition of coatings. *Progress in material Science*, 57-170.

Clarke, D., Oechsner, M., & Padture, N. (2012, October Vol 37, No 10). Thermal-barrier coatings for more efficient gas turbines. *MRS Bulletin*. Materials Research Society.

Cosack, T., & Schultz, U. (2012). *Mass production and future aspects for EBPVD thermal barrier caotings.* Munich/ Germany: MTU Aero Engines.

HASS, D., SLIFKA, J., & WADLEY, H. (2001). *LOW THERMAL CONDUCTIVITY VAPOR DEPOSITED ZIRCONIA MICROSTRUCTURES.* Charlottesville: National Institute for Standards and Testing, Materials Reliabilit.

Hayashi, H., Saitou, T., Maruyama, N., Inaba, H., & Kawamura, K. (2005). Thermal expansion coefficient of yttria stabilized zirconia for various yttria contents. *Solid State Ionics*, 631-319.

Hoshyarmanesh, H. (2014, 03 25). *PRATT & WHITNEY JT3D, JT8D, JT9D ENGINE FAMILIES*. Retrieved from Cirrus Aviation inc.: http://cirrusaviationinc.com/jt8d.htm / https://grabcad.com/library/shrouded-turbine-blade-pratt-whitney-standard

Jenoptik. (2014, 04 11). *HOMMEL-ETAMIC T8000 RC*. Retrieved from Jenoptik Industrial Metrology: http://www.jenoptik.com/Internet_EN_HOMMEL-ETAMIC_T8000_RC

Kemp, J. (2014, 04 21). *Standard deviation diagram.* Retrieved from Wikipedia: http://en.wikipedia.org/wiki/Standard_deviation#mediaviewer/File:Standard_deviation_diagram.svg

Kolkman, H. (1987). Creep, Fatigue and Their Interaction in Coated and Uncoated Rene 80. *Mat.Sci.Eng 89*, 81-91.

Lau, H. L. (2003). Influence of bondcoat pre-treatment and surface topology on the lifetime of EB-PVD TBCs. *Surface and Coatings Technology*, 217-223.

Lowrie, R., & Boone, D. (1977). Composite coatings of CoCrAlY plus platinum. *Thin Solid Films*, 491-498.

Mahomed, N. (2013, September). Email correspondence. *Email correspondence.*

Miller, R. A. (2009). History of Thermal Barrier Coatings for Gas Turbine Engines. *Emphasizing NASA's Role From 1942 to 1990.* Ohio: NASA.

Nicholls, J. (2003). Advances in Coating Design for High Performance Gas Turbines. *MRS Bull*, 659-670.

Okazaki, M. (2001). High-temperature strength of Ni-base superalloy coatings. *Science & Technology of Advanced Materials*, 357-366.

Osorio, J., Toro, A., & Hernandez-Ortiz, J. (2012). *THERMAL BARRIER COATINGS FOR GAS TURBINE APPLICATIONS: FAILURE MECHANISMS AND KEY MICROSTRUCTURAL FEATURES.* Medellín: Universidad Nacional de Colombia.

Pierson, H. (1999). *Handbook of chemical vapor deposition (CVD). Principles, Technology & Applications. Second Edition.* New York: Noyes Publications.

Reed, R. (1997). *Heat-Resistant Materials, ASM International.* Ohio, USA: ASM.

Research and Development Laboratory for Aerospace Materials, M. (2014). Laboratory Pictures. Rzeszow, Poland: Research and Development Laboratory for Aerospace Materials.

Rumsey, D. (2011). *Statistics for Dummies, 2nd edition.* John Wiley & Sons.

Sampath, S., Schultz, U., Jarligo, M., & Kuroda, S. (2012). Processing science of advanced thermal-barrier systems. *MRS Bulletin*, 903-909.

Sastry, M. D. (2012). Analysis and optimization of machining process parameters using design of experiments. *Industrial Engineering Letters*.

Schulz, U., Munawar, A., & Mechnich, P. (2012). Advanced EB-PVD Thermal Barrier Coatings for Turbine Applications. *Symposium at Politechnika Rzeszow 21-24.10. 2012.* Rzeszow.

Slawomir, K. (2013). Advanced Technologies for Aerospace Industry. *Official presentation of the Research and Development Laboratory For Aerospace Materials at the Rzeszow University of Technology.* Rzeszow, Poland.

Sou, Z. (2002). Reliability of Interconnect Structures. *Comprehensive Structural Integrity, Volume 8: Interfacial and Nanoscale Failure*.

Special-Metals. (2014, 06 10). *INCONEL® alloy 617*. Retrieved from Special Metals: file:///C:/Users/Maximus/Desktop/Inconel%20alloy%20617.pdf

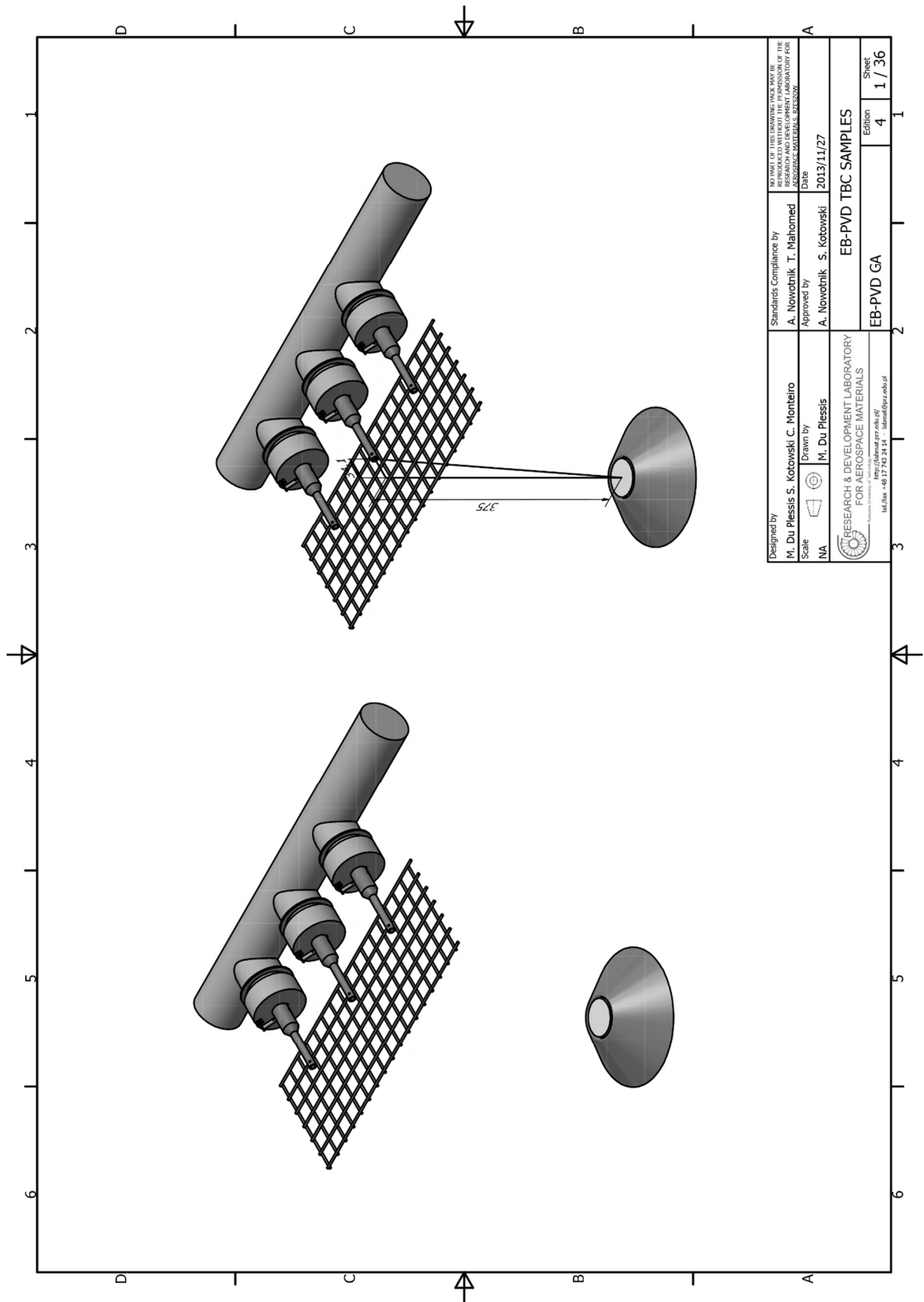Sun, W., Lin, H., & Hon, M. (1986). CVD Aluminide Nickel. *METALLURGICAL TRANSACTIONS*, 220-226.

Vaidyanathana, K., Jordanb, E., & Maurice, G. (2004). Surface geometry and strain energy effects in the failure of a (Ni, Pt)Al/EB-PVD thermal barrier coating. *Acta Materialia volume 52*, 1107–1115.

Walters, C. (2005). *Simulation of Diffusion Processes in Turbine Blades and Large Area Deposition of MAX Phase Thin Films with PVD.* Aachen: Von der Fakultˇat fˇur Georessourcen und Materialtechnik der Rheinisch-Westfˇalischen Technischen Hochschule Aachen.

Warnes, B. (2003). Improved aluminide/MCrAlX coating systems for super alloys using CVD low activity aluminizing. *Surface and Coatings Technology*, 106-111.

Yuan, K. (2013). *Thermal and Mechanical Behaviors of High Temperature Coatings.* Linköping: Linköping University.

Yuan, K., Erikson, R., Peng, R., Li, X., Johanson, S., & Wang, Y. (2013). *Modeling of the microstructural evolution and lifetime prediction of MCrAlX coatings on Nickel based superalloys in high temperature oxidation.* Linköping: Linköping University, The Institute of Technology.

Zhang, Y., Withers, P., Fox, M., & Knowles, D. (1999). Damage mechanisms of coated systems under thermomechanical fatigue. *Materials Science and Technology*, 1031-1036.

Appendices

A CAD draft of AISI314 wire mesh
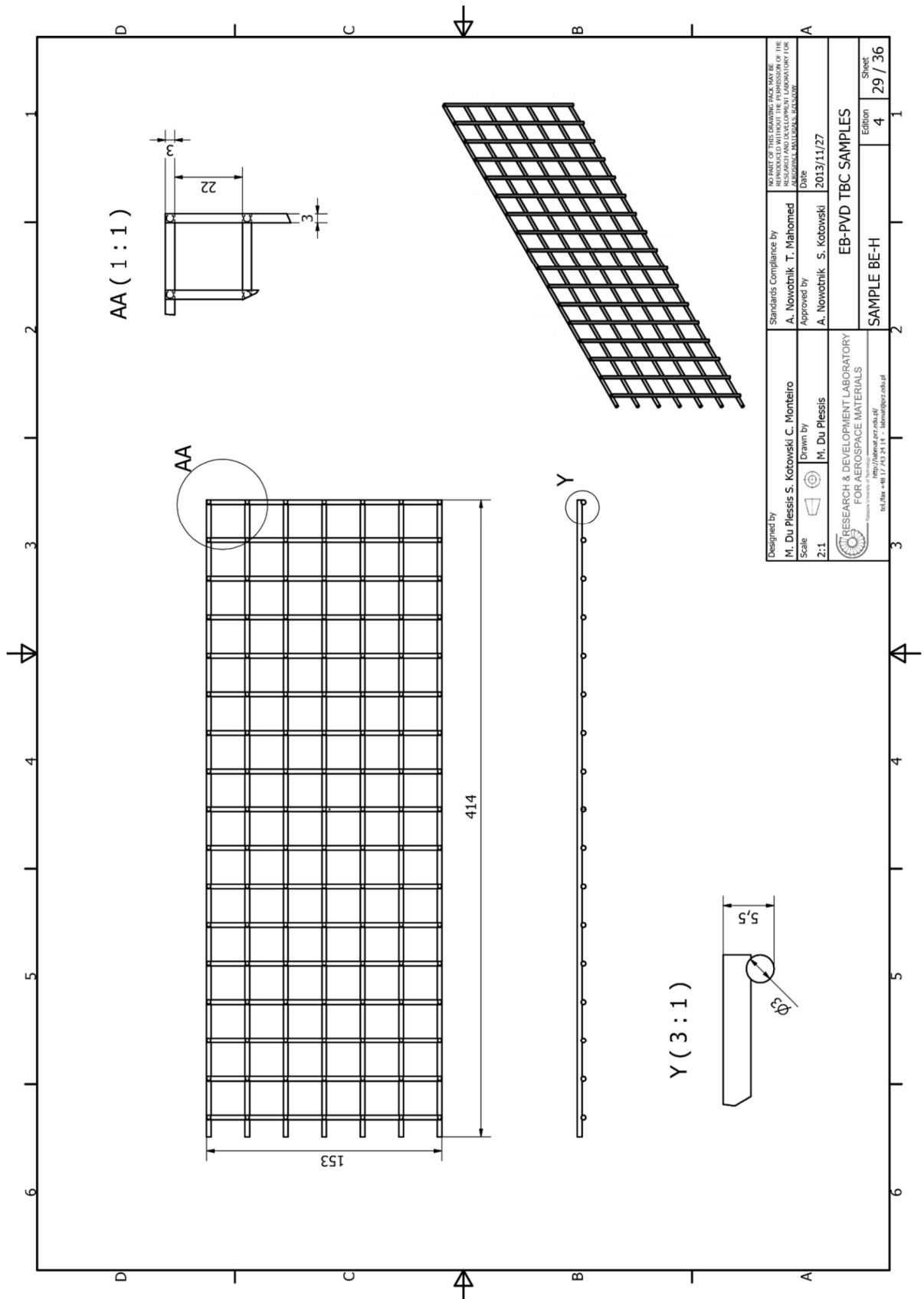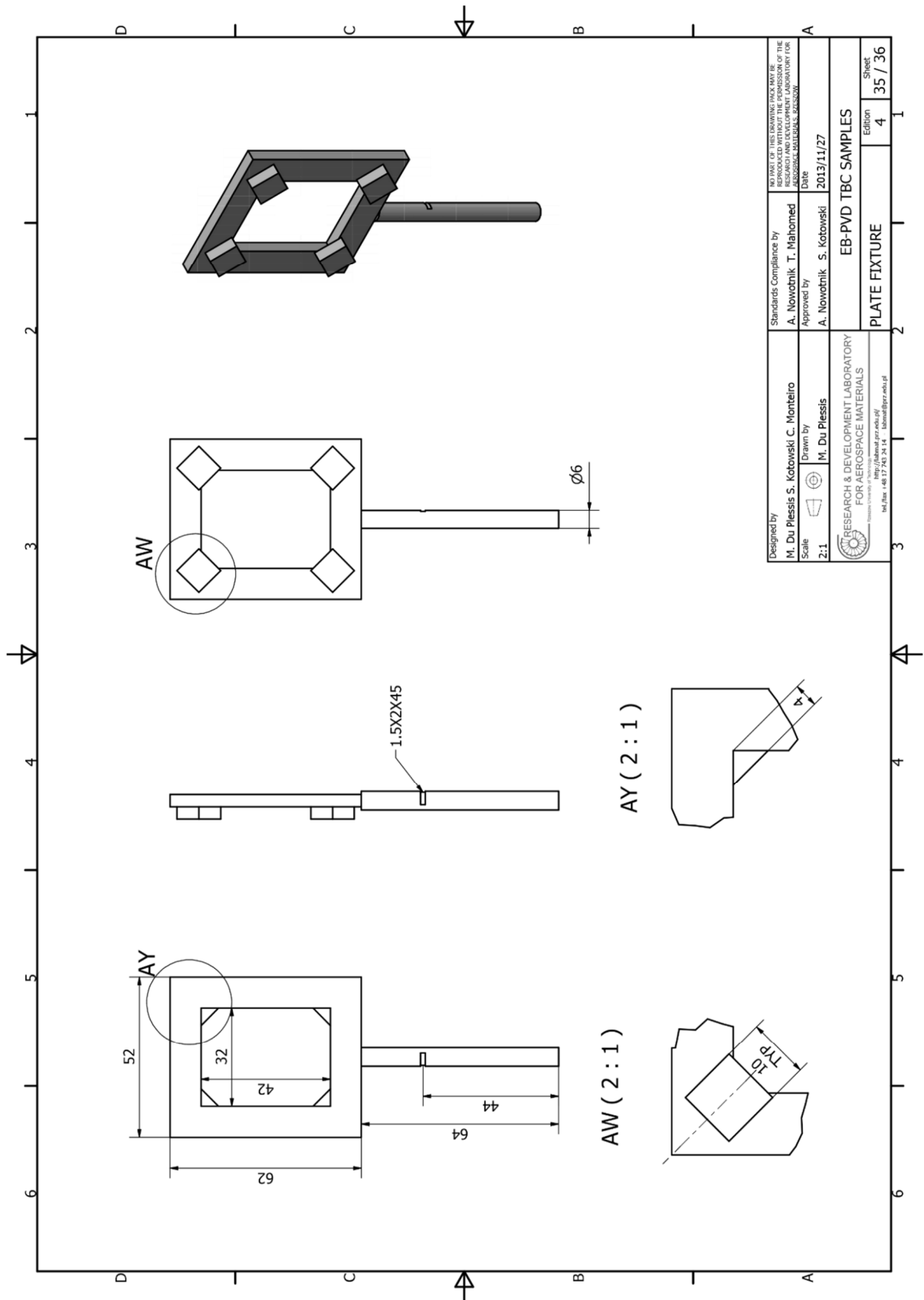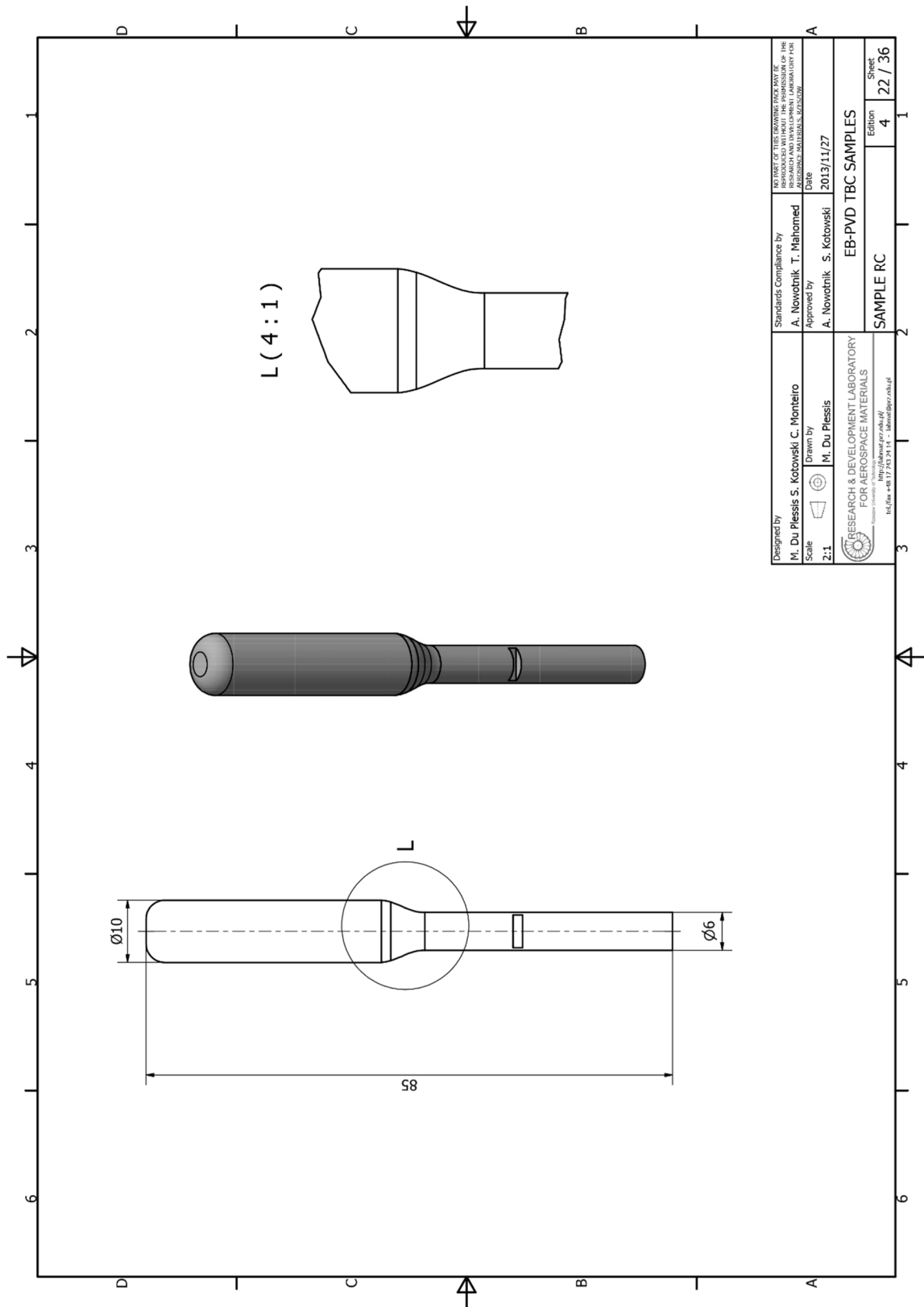
B Location of AISI314 wire mesh relative to evaporator

C CAD draft of Inconel617 flat sample

D CAD draft of Inconel617 flat sample fixture

E CAD draft of Inconel617 Cylindrical sample fixture

L (4 : 1)

Ø10

Ø6

85

L